12-2022

Effects of Fibers in Dense Graded and Gap Graded Asphalt Concrete

Franher Daniel Cantu
The University of Texas Rio Grande Valley

EFFECTS OF FIBERS IN DENSE GRADED AND GAP GRADED ASPHALT CONCRETE

A Thesis

by

FRANHER DANIEL CANTU

Submitted in Partial Fulfillment of the

Requirements for the degree of

MASTER OF SCIENCE

Major Subject: Civil Engineering

The University of Texas Rio Grande Valley

December 2022

EFFECTS OF FIBERS IN DENSE GRADED AND GAP GRADED ASPHALT CONCRRETE

A Thesis
by
FRANHER DANIEL CANTU

COMMITTEE MEMBERS

Dr. Philip Park
Chair of Committee

Dr. Thang Pham
Committee Member

Dr. Mustapha Rahmaninezhad
Committee Member

December 2022

ABSTRACT

Cantu, Franher D., Effects of fibers in Dense Graded and Gap Graded Asphalt Concrete. Master of Science (MS), December, 2022, 80 pp., 1 table, 59 figures, references, 53 titles.

As a part of efforts to understand the interactions between fibers and particles in compliant binder such as asphalt. This investigated the compressive behaviors of fiber reinforced asphalt concrete with different aggregate gradation, such as gap graded and dense graded. There have been multiple studies attempting to understand the impact of fibers on particle reinforced composites, however, only few of those focused on the fiber-particle interactions. A comprehensive literature review on the current state of the art of fiber reinforced asphalt concrete and fiber-particle interactions was conducted. Then a series of compression tests were conducted using various size steel fibers and polyvinyl alcohol fibers for dense graded and gap graded (stone matrix) asphalt concrete. The results show that adding fibers increases air voids and correspondingly reduces the compressive strength and stiffness but increases the pre- and post-cracking energy. These behaviors were observed in both dense and gap graded asphalt mixtures.

DEDICATION

This thesis is dedicated to my family and to my friends that have supported me in many ways. I would like to thank my parents, B. Homero Cantu and Zoraya I. Cantu for their incredible support, and to my girlfriend, Dora K. Conover, that has been with me throughout this journey. I could not have accomplished any of this without you. Thank you.

ACKNOWLEDGMENTS

I would like to thank Dr. Philip Park for the guidance, teachings, support, and mentorship. I am thankful for this opportunity and for trusting me to collaborate with you for the past three and a half years. I would also like to thank Mateo Schmit-Mendoza and Leonardo Ortega for assisting me in this project.

Additionally, I would like to thank the Valero Energy Corporation for providing the asphalt binder needed to accomplish this project. Finally, I would like to thank the Civil Engineering department here at UTRGV for providing the facilities and resources to accomplish this project.

TABLE OF CONTENTS

Page

ABSTRACT iii

DEDICATION iv

ACKOWLEDGMENTS v

TABLE OF CONTENTS vi

LIST OF TABLES viii

LIST OF FIGURES ix

CHAPTER I. INTRODUCTION 1

Justifications and Background 2

Problem Statement 3

Objective of Research 5

CHAPTER II. LITERATURE REVIEW 6

Fiber-Aggregate Interaction 6

Previous Use of Fibers 12

Mechanical Performance of FRAC 21

CHAPTER III. EXPERIMENTAL PREPARATIONS 28

Material Acquisition 28

AASHTO Standards 33

Preparations and Asphalt Mixing 47

Loading Equipment 52

CHAPTER IV. RESULTS AND DISCUSSION 54

Test Results 54

Discussion 70

CHAPTER V. CONCLUSIONS AND FUTURE WORK 75

REFERENCES 76

BIOGRAPHICAL SKETCH 80

LIST OF TABLES

Page

Table 4.1: Key values obtained from each specimen..... 59

LIST OF FIGURES

Page

Figure 2.1: Schematic view of the fiber reinforcing mechanism with a compliant binder (Park et al. 2015) 8

Figure 2.2: Load deformation curve of square concrete panels: (a) 10 mm maximum aggregate size and (b) 20 mm maximum aggregate size (Ige et al. 2017) 9

Figure 2.3: Asphalt concrete without fibers (left) and with fibers (right) (Noorvand et al. 2021) 10

Figure 2.4: Results of the Uniaxial Fatigue test. (Noorvand et al. 2021) 11

Figure 2.5: Comparison of pull-out force–displacement curves of different failure modes (Park et al. 2017) 14

Figure 2.6: Relationship between the temperature of the test and ITS and FE responses for both ypes of fiber (Slebi-Acevedo et al. 2020) 15

Figure 2.7: Results of the mix design for fiber-reinforced hot mix asphalt mixtures using the 15 s dispersion and dry mixing methods: (a) Rice specific gravity (Gmm), (b) bulk specific gravity (Gmb), (c) air void content (AVC), (d) voids in mineral aggregate (VMA) (Alfalah et al. 2020) 16

Figure 2.8: Test results for unreinforced and fiber-reinforced hot mix asphalt mixtures: (a) dynamic complex modulus, |E*|, master curves and (b) Cantabro loss (Alfalah et al. 2020) 17

Figure 2.9: Ultimate tensile strain of distinct groups (top left), Ultimate tensile stress of different groups (top right), and Cracking energy of different FRAC mixtures (bottom) (Guo et al. 2020) 18

Figure 2.10: Represents the results of the Ultimate Flexural Strain of FRAC of several types of fibers (Xu et al. 2010) 20

Figure 2.11: Flexural Stress vs Strain curves for several binder contents and different temperatures (Yang et al. 2016) 21

Figure 2.12: Influence of steel fiber content on the stability (top) and bending tensile strength of asphalt concrete under different temperature, different content of steel (bottom) (Guo 2014) 23

Figure 2.13: The radar charts for five types of asphalt mixture (Liu et al. 2021) 24

Figure 2.14: Accumulated strain during flow number test (Noorvand et al. 2018).....25
Figure 2.15: Gradation curves for SMA-13 (a), SUP-13 (b), SUP-20 (c), SUP-25 (d) (Lou et al. 2021) 27
Figure 3.1: Blue limestone used for the research.....30
Figure 3.2: Pulverized sand used for the research 31
Figure 3.3: Asphalt Aggregate Gradation Curve 31
Figure 3.4: Fibers used in this Experiment 32
Figure 3.5: Metallic Volumetric Flask.....34
Figure 3.6: Appropriate connections from volumetric container to pump 34
Figure 3.7: Air pump.....35
Figure 3.8: Electronic auto-rice controller.....35
Figure 3.9: Water bath equipment setup 36
Figure 3.10: Air void removal equipment setup 36
Figure 3.11: Metallic Cone and Tamper 40
Figure 3.12: Pycnometer with a capacity of 1000ml 42
Figure 3.13: Gilson Co. Superpave Gyratory Compactor.....45
Figure 3.14: Asphalt Compaction Mold 46
Figure 3.15: Mechanical Sieve Shakers.....48
Figure 3.16: Metallic Asphalt Containers.....50
Figure 3.17: Asphalt mixing apparatus.....51
Figure 3.18: MTS Machine.....53
Figure 4.1: Air Voids to Fiber Percentages 55
Figure 4.2: Stress Strain Curve for DG Hooked Steel Fibers. 56
Figure 4.3: Stress Strain Curve for DG Large Hooked steel Fibers. 56
Figure 4.4: Stress Strain Curve for DG PVA Fibers.....57
Figure 4.5: Stress Strain Curve for SMA Hooked Steel Fibers 57
Figure 4.6: Stress Strain Curve for DG under different Temperatures.....58
Figure 4.7: Stress Strain Curve for SMA under different Temperatures.....58
Figure 4.8: Toughness of DG Hooked Steel Fibers. 60

Figure 4.9: Toughness of DG Large Hooked Steel Fibers.....60
Figure 4.10: Toughness of DG PVA Fibers. 61
Figure 4.11: Toughness of SMA Hooked Steel Fibers. 61
Figure 4.12: Toughness of DG FRAC under different temperatures.....62
Figure 4.13: Toughness of SMA FRAC under different temperatures.....62
Figure 4.14: Peak stress to Fibers (DG).....63
Figure 4.15: Peak stress to Fibers (SMA).....63
Figure 4.16: Peak stress to Air Voids (DG).....64
Figure 4.17: Peak stress to Air Voids (SMA).....64
Figure 4.18: Cracking Energy to % Fibers DG.....65
Figure 4.19: Post-Cracking energy to % Fibers DG.....65
Figure 4.20: Cracking Energy to % Fibers SMA.....66
Figure 4.21: Post-Cracking energy to % Fibers SMA.....66
Figure 4.22: Cracking Energy to Air Voids % DG.....67
Figure 4.23: Post-Cracking energy to Air Voids % DG.....67
Figure 4.24: Cracking Energy to Air Voids % SMA.....68
Figure 4.25: Post-Cracking energy to Air Voids % SMA.....68
Figure 4.26: Cracking energy, and Post-Cracing Energy (Park et al. 2015) 69

CHAPTER I

INTRODUCTION

Fiber Reinforced Asphalt Concrete (FRAC) is a composite that is composed of fibers, various size particles (aggregate), and compliant binder (asphalt). The mechanical behavior of asphalt binder is highly dependent on loading rate and temperature: the binder becomes more compliant in high temperatures and slow loading rates than cold temperatures and fast loading rates. Since the compliant binder does not have sufficient binding force to hold fibers under loads, the reinforcing effect of fibers would not be significant in room temperature or above. In this case, the interlocking of fibers in aggregates can play a critical role in improving reinforcing effects.

It is well known that the coarse aggregates in asphalt concrete form a skeletal structure through stone-on-stone contacts and the skeletal structure carries most of compressive force. Fibers interlocked between the skeletal system allows the material to have desirable or improved cracking and rutting resistances. However, to activate this reinforcing mechanism, the selection of fiber dimension and material that matches with aggregate size and gradation would be very important. Fibers don’t only interact with the aggregate, but also with the binder, so to effectively measure the fiber-aggregate interaction, the fiber-binder interaction must be isolated from the experiment.

Justifications and Background

Because of its mechanical performance, ability to rehabilitation, user comfortability, and recyclability, asphalt concrete has become the most preferable material for paving roads. Currently there are more than 2.6 million lane miles of asphalt roads in the US. Therefore, maintaining the quality of these roads have become a significant burden of federal and local government budgets. Currently, measures to improve the service life of asphalt pavements have been studied in various approaches.

Early fiber reinforced structures were recorded in China, where some arches were made of clay mixed with what is natural fibers. Previously, during the Egyptian and Mesopotamian times (early 1500 BC), fiber reinforced composite materials were used to construct structures. These materials were typically composed of mud and straw that were durable and strong enough to create buildings. Straw was able to produce enough reinforcement to create a variety of structures, such as pottery and boats. Studies have shown that the straw reinforcement allowed the bricks to dry more evenly, thus preventing cracking in the materials during the construction process (Vargas-Neumann et al. 1986). Modern uses of fibers have been investigated since the early 1960s (Mahrez et al. 2003). Since then, a large variety of fibers have been introduced and studied. Recently, a variety of synthetic, metallic, and natural fibers have been used to modify the performance of composite materials. Slebi-Acevedo et al. (2019) analyzed various types of synthetic and metallic fibers and was able to determine significant improvement in the composite material.

Asphalt concrete is a flexible composite material that is made of bitumen and aggregates. Compared to concrete or other engineering materials, asphalt is a weak material. Vehicle loads can cause fatigue, rutting, and other types of failures in asphalt pavements (Abtahi et al. 2010).

Because of problems like this, extensive research on fiber reinforcements to improve the mechanical performance and corresponding economic viability of asphalt pavements has been studied. Zube (1956) was the earliest recorded study of the uses of a type of modern fiber reinforcement in asphalt concrete. Zube used wire mesh to an asphalt pavement. He tested a variety of meshes in the bituminous surfacing. Zube concluded that all wire meshes reduced cracking and improved the mechanical performance of the asphalt concrete. He also concluded that because of its mechanical improvement, the thickness of the overlay can be reduced.

Park et al. (2015) discusses the role of the fiber-binder adhesion and fiber-aggregate interlocking in fiber pullout tests in asphalt. So far, not many papers discuss the interlocking between fibers and aggregate and how mechanical performance is affected. Ige and Barnett (2017) investigate the behavior of fibers, aggregate size, and aspect ratio of the fibers. Using concrete as a binder, he discovered that the smaller (10mm) aggregates performed better in an IDT test than larger (20mm) aggregates. Unfortunately. the possibility of interlocking is not discussed. Yoo et al. (2017) explored the relationship between the fiber pullout strength and the strength of the matrix. This experiment was conducted using a type of High-performance fiber-reinforced cementitious composite (HPFRCC). Two fibers were tested, straight and hooked end steel fibers. He concluded that when the strength of the matrix was improved so was the pullout strength of the fiber.

Problem Statement

To maintain roads that withstand loads from large vehicle and truck loads, modern asphalt pavements must be designed accordingly to maintain the standard service life.

Rehabilitation of asphalt pavements have become a substantial expense for local and federal transportation agencies. Because of this, many roads are started to be paved with concrete, however concrete pavements cause large initial costs and an environmental cost. Current research has attempted to improve the mechanical properties of asphalt concrete to withstand loads for longer service life and reduce maintenance costs.

Modern research has explored the use of fibers in asphalt concrete to improve the stability. Fibers have been used to prevent draindown or to improve the mechanical performance. Fibers interact with the aggregate and the binder to provide these qualities. Former studies on FRAC have shown discrepant results: some reported significant improvements and others reported no improvements. The lack of understanding on the fiber aggregate interlocking might be the possible reason of this discrepancy.

Park et al. (2015) suggested a hypothesis on the fiber-particle interaction in fiber-particle reinforced composites with compliant binders. Park et al. stated that if fibers interlocked between the particles forming a skeletal structure, it will provide substantial reinforcing effects. To investigate the fiber-aggregate interlocking mechanism, an experimental program comparing asphalt concrete with and without fibers, fibers with various lengths, thicknesses, and stiffnesses, and diverse maximum aggregate sizes and gradations is needed. Temperature is another important parameter for the investigation since the behavior of asphalt concrete highly depends on temperature. In many states, different types of binders are used depending on the climate they face. This study cannot cover all the complex variables but will provide fundamental background information for understanding the fiber-particle interactions in asphalt concrete.

Objective of Research

As a part of the research to understand the fiber-particle interaction, this study aims to investigate the effects of fiber type, length, and aggregate gradation on the fiber-particle interaction in a limited range. A comprehensive literature review was conducted on fiber reinforced asphalt concrete. Papers regarding the interaction between fibers and the skeletal structure of the material were reviewed. In the experimental program, compressive stress-strain curves were obtained from various the asphalt concrete specimens listed below:

- Dense graded asphalt concrete without fibers (control, NMAS 12.5 mm)
- Dense graded asphalt concrete reinforced with 30 mm long steel fibers
- Dense graded asphalt concrete reinforced with 40 mm long steel fibers
- Dense graded asphalt concrete reinforced with 30 mm long polyvinyl alcohol (PVA) fibers
- Gap graded asphalt concrete without fibers (control, NMAS 19 mm)
- Gap graded asphalt concrete reinforced with 30 mm long steel fibers

Most of the tests were conducted at room temperature (20 °C), and the tests for high service temperature (60 °C) and low service temperature (-20 °C) were conducted for selected cases. The results of these tests will provide the basic information to understand fiber-aggregate interaction in asphalt concrete.

CHAPTER II

LITERATURE REVIEW

In this literature review the interaction between aggregates and fibers will be discussed. Fiber interlocking and its effects will be explored in composite materials, this includes all the studies done to the date of this paper. Other types of fibers will be discussed and how they interact with the skeletal structure, the impact will be measured through various types of tests on the specimen and their results. Finally, the mechanical performance of FRAC will be explored. Here, expectations for the results will be made and through that the success of the research. Except for the analysis of the fiber-aggregate interactions, the other collections of literature will be done using exclusively asphalt, this is because there is not much analysis exploring the fiber-aggregate interlocking using asphalt, most studies have used fiber reinforced concretes.

Fiber-Aggregate Interaction

A composite is a multiphase material that is classified into components. These components are continuous phase and the dispersed phases. The binder or matrix within the composite is the continuous phase, while the particles or the fibers within are an additional reinforcement and is part of the dispersed phase. The reinforcement is used to bind the material together and to transfer the loads within the member. A compliant binder such as asphalt concrete will allow us to test the fiber-aggregate interlocking. When a compressive load is

applied, the force is distributed through the skeletal structure through stone-on-stone contact. When fibers are added, this mechanism should improve, giving the asphalt concrete desirable material properties. In the case of fiber reinforced concrete, the stiff binder will not use this mechanism. Fibers in the stiff binder will only interact with the binder through friction and adhesion, rather than the entire skeletal structure. Tahenni et al. (2016) addresses the importance of the bond strength between the concrete and the fibers to maintain the benefits provided. The strength of the fibers within the skeletal structure depends on the fiber's interaction with the binder and the aggregate. Mohammed et al. (2018) explores how fibers can help improve these interacting mechanisms. Additional interactions might be affected by the fiber's aspect ratio, i.e., diameter (Kim et al. 2018; Pei et al. 2021) and length.

Park et al. (2015) discusses the effects of the fibers in the skeletal structure of the asphalt concrete. An interaction between the fiber, aggregate, and binder was discussed. Figure 2.1 shows a schematic view of the reinforcing mechanism. When the skeletal structure is under compressive loads, the stone-on-stone contact and fibers create a scenario where the fiber is wedged between the aggregate. The geometry of the fiber plays a crucial role in this mechanism. The longer the fiber, the probability of the fiber interlocking with more particles is greater. The thickness of the fiber may allow the fiber to withstand and transfer higher loads. Shorter and thin fibers might have negative or negligible effects on the skeletal structure. By improving the interlocking mechanism, crack remediation and strength of the material is improved.

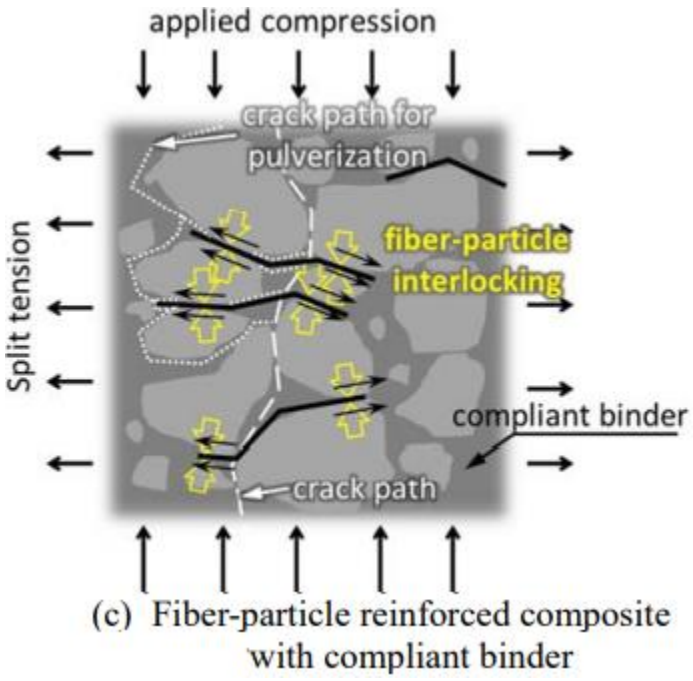

Figure 2.1: Schematic view of the fiber reinforcing mechanism with a compliant binder (Park et al. 2015).

Ige et al (2017) explores and tested the interaction between steel fibers and aggregate in fiber reinforced concrete. This scenario utilizes a stiff binder with multiple sizes of aggregates and various fiber dimensions to see how the mechanical behavior is impacted. Compression tests are performed on concrete samples to test their theory. The test did result in conclude that the concrete with smaller size aggregates and larger aspect ratio of fibers were able to withstand more deflection and load capacity than the larger aggregates. Figure 2.2 shows the load deformation curve of the concrete samples, where the top numbers are the aspect ratio/length respectively.

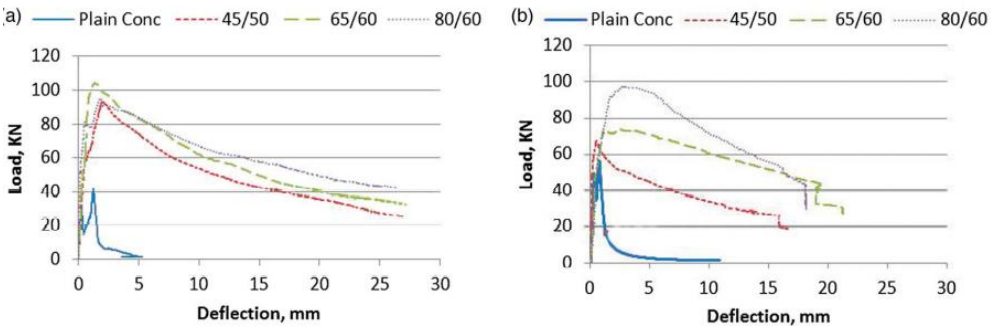

Figure 2.2: Load deformation curve of square concrete panels: (a) 10 mm maximum aggregate size and (b) 20 mm maximum aggregate size (Ige et al. 2017).

However, this analysis does not measure interlocking or how the smaller sized aggregate could have interacted with the fibers. It analyzes the impact of the size of aggregate and the dimensions of the fiber independently and how they both impact the overall performance of the member.

Slebi-Acevedo et al (2019) noted that the fiber-aggregate interconnection allowed the material to withstand more strain energy before cracking. He also analyzed the microstructure of the asphalt, and noted that the shape, dimension, and quantity of fiber were a crucial factor in the skeletal structure of the asphalt. He claims that the fibers can form a network with the asphalt, resulting in stronger connections that lowered the risk of crack propagation. Through the fiber-aggregate interlocking, roads lifecycle is extended. This author also explores the benefit of fiber interlocking to form a better networking system.

One of the most typical problems with asphalt pavement is cracking. Synthetic fibers have been demonstrated to strengthen asphalt concrete's tensile strength, which lowers the likelihood of cracking because asphalt concrete is weak in tension.

Noorvand et al. (2021) evaluates the impact that the fiber length has on asphalt concrete. This paper is reminiscent of the previously discussed paper by Park et al. (2015), where this bridging effect is discussed. This paper studies the relationship between fibers and asphalt mastic as well as the dispersion of fibers in asphalt concrete. Two varieties of nylon fiber and three varieties of aramid fiber were employed in this experiment. Shear binding strength between the fibers and the asphalt mastic was assessed using a fiber pullout test. Following the pullout test, the bond strength was used to determine the minimum length of fiber that must be embedded on either side of the fracture for the fiber to reach its full capacity before being taken out. The paper stated that longer fibers affected dispersion. According to the study, aramid fibers of around 20 mm in length would produce a satisfactory bond with asphalt mastic and allow for adequate dispersion in the FRAC. Additionally, the flow number test and the uniaxial fatigue test were carried out on FRAC with various aramid fiber lengths. Also, performance test findings for the 19-mm fibers were superior to those for the 10- and 38-mm fibers.

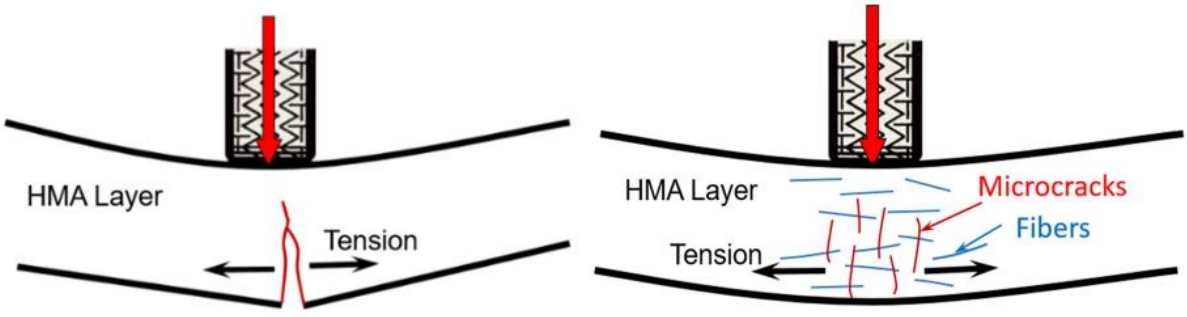

Figure 2.3: Asphalt concrete without fibers (left) and with fibers (right) (Noorvand et al. 2021).

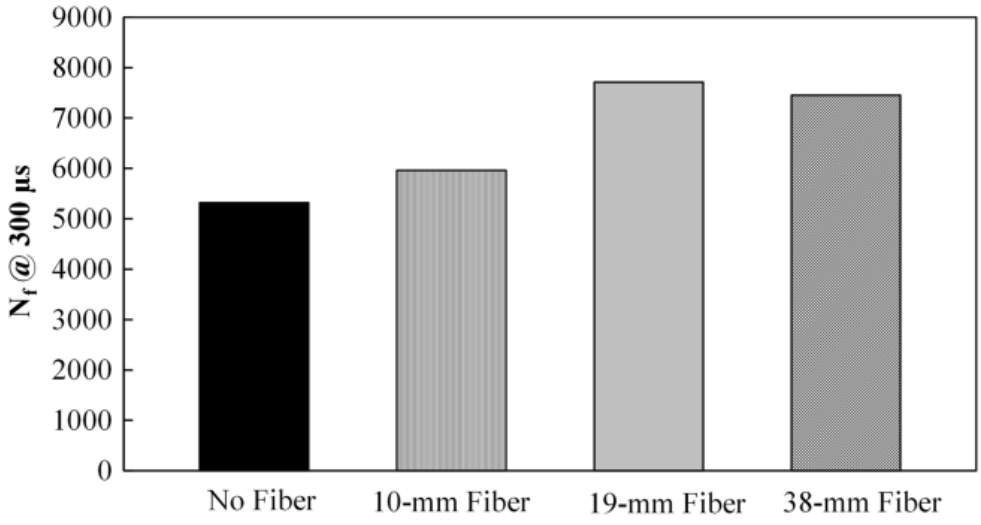

Figure 2.4: Results of the Uniaxial Fatigue test. Results of the different fiber lengths (Noorvand et al. 2021).

Yoo et al. (2017) determined whether the flexural behavior of high-performance fiber reinforced cementitious composites (HPFRCC) and single fiber pullout behavior were correlated. Three different matrix strengths and two distinct steel fiber types were observed, this included straight and hooked steel fibers. According to test results, increasing matrix strength led to better fiber pullout performance. The bond strengths and pullout work of the hooked fibers were higher than those of the straight fibers, although at large slips, the shear stress at the interface was lower than that of the straight fibers. The best flexural performance was demonstrated by beams with medium-length straight fibers, whereas the worst performance was demonstrated by beams with hooked fibers.

Previous Use of Fibers

One aspect of the interlocking mechanism is assumed to be achieved through the stiffness of the fiber and the ability to wedge itself through the aggregate. It is predicted that steel fibers have the required material properties to access the interlocking mechanism within the skeletal structure. As previously mentioned, using fibers as a reinforcing material has allowed for better material performance (Mashaan et al. 2021). However, different fibers improve different aspects of the material, so in this section different types of fiber material will be discussed and what was able to be accomplished with that fiber. There are several factors that contribute to the effectiveness of the fibers. Alfalah et al. (2021) evaluates the impact that fiber content and fiber type have on the mechanical performance of AC. Insufficient fibers can be found to be ineffective, while excessive quantities of fibers ca be harmful to the overall performance of the AC. Serin et al. (2012) studied the impact that adding fibers can have on binder content. The author eventually concluded that a 0.75% steel fibers withs a 5.5% bitumen content performed the best. This paper reinforces the idea of selecting the optimum quantity of fibers in the asphalt mixture. Several fiber materials have been studied to determine the most effective way to implement the use of fibers in asphalt projects. This optimum fiber content might vary for every project, Muftah et al. (2017) recommends evaluating different fiber contents for the asphalt mixture or in many cases using the content recommended by the manufacturer. These fiber types can include glass (Mahrez et al. 2003; Mahrez et al. 2005; and Enieb et al. 2021), basalt (Cetin et al. 2021 and Xingyu et al. 2013), steel, synthetic (Chen et al. 2009 and Kim et al. 2018), and even natural fibers (Keya et al. 2019). Each fiber type varies in cost, mixing capabilities, asphalt binder compatibility, and mechanical improvements.

Park et al. (2017) observed the behavior of steel fibers through fiber pull out tests from the asphalt matrix. Various scenarios with different temperatures, displacement rates, and fiber dimensions were tested. Results were categorized under 3 different, pull-out failure modes: matrix, interface, and a mixed failure. The matrix failure mode (MaF) occurs when the asphalt where the fiber is embedded with is pulled out with the fiber. The MaF commonly occurred under higher temperatures and at a slower pull-out speed. The interface failure (InF) occurs when the fiber is completely separated from the binder. This most occurred under lower temperatures and higher pull-out speeds. Finally, the mixed mode failure (MMF) occurs when the fiber is separated from the fiber but partially contains some asphalt on one side. As this implies, this is a combination of interface and matrix failures. Overall, this experiment determined that longer fibers performed better under lower temperatures when the ductility was tested, and shorter fibers performed better in rutting resistance.

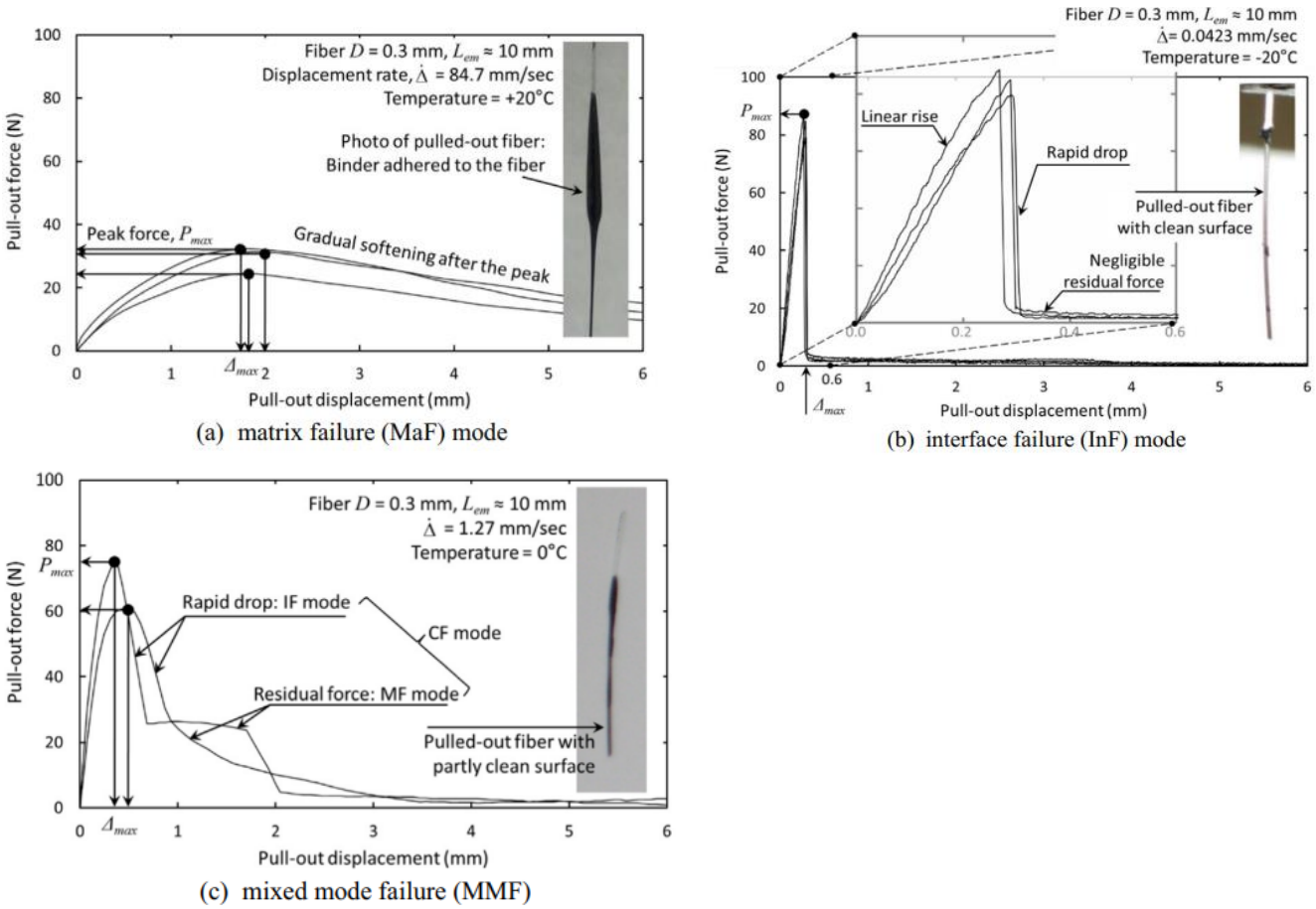

Figure 2.5: Comparison of pull-out force–displacement curves of different failure modes (Park et al. 2017).

Slebi-Acevedo et al. (2020) research the impact of synthetic fibers under different temperatures and fiber contents in asphalt specimens. The synthetic fibers used in this experiment were polyolefin-aramid (POA) and polyacrylonitrile (PAN) fibers. The fiber content used were tested in percentage by weight at 0.1%, 0.2%, and 0.3% at -15ºC, 0ºC, and 15ºC. Indirect tensile strength, Cracking energy, post-cracking energy and toughness were the parameters used to measure the performance of the synthetic fibers and fiber content. Unfortunately, there were no major improvements in the use of synthetic fibers in this experiment. The author claimed that there were improvements in with the use of fibers, but that it

was not significant enough to claim that the use of these synthetic fibers improved the performance of the asphalt. The author does not explore the reason these fibers were unable to improve the performance of the asphalt specimens.

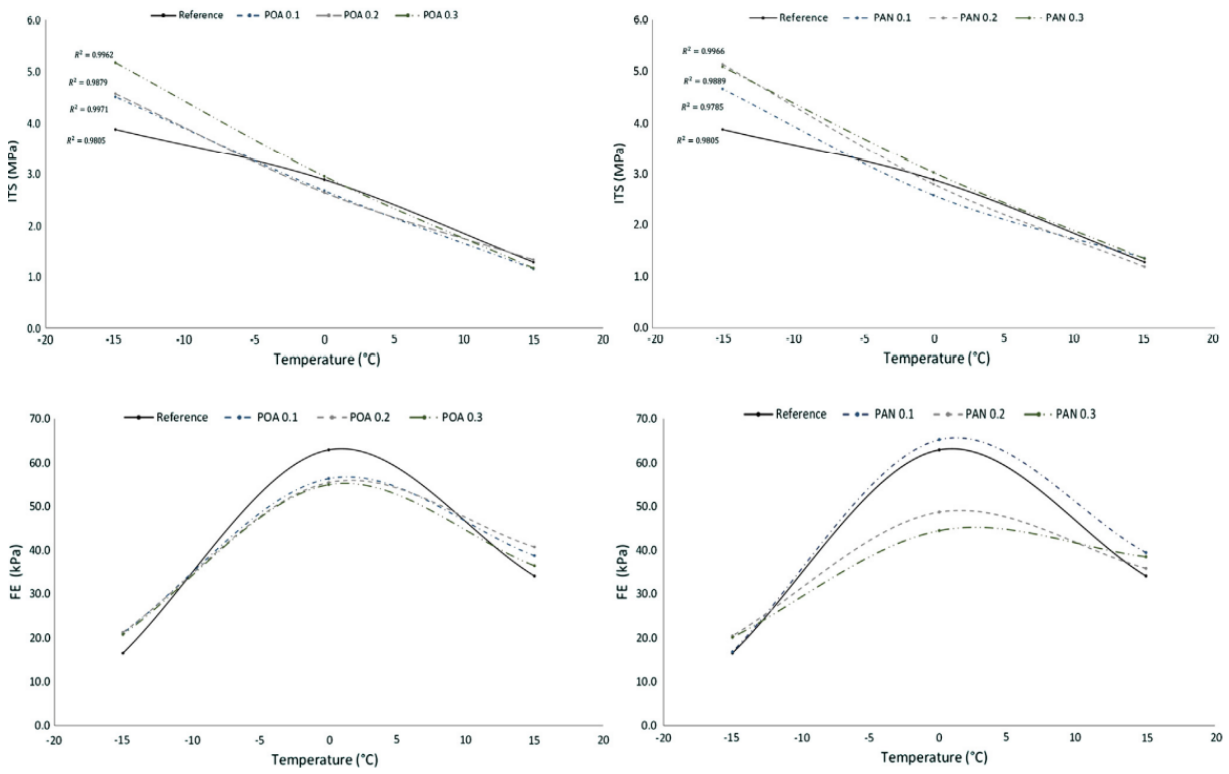

Figure 2.6: Relationship between the temperature of the test and ITS and FE responses for both types of fiber (Slebi-Acevedo et al. 2020).

Alfalah et al. (2020) attempts to evaluate and compare the performance of multiple types of fibers in HMA. Three types of fiber reinforcement were used: fiberglass, basalt, carbon, and polyolefin/aramid blend. The fiber content remained constant for the respective fiber type. The authors emphasized the importance of mixing the way the fibers were mixed into the asphalt. A 15-sec dispersion method and a dry method were used in this investigation. In the dry method all the fibers are mixed with the aggregate before the addition of the binder. While in the 15-sec method, the fibers were introduced into the mixture every 15-seconds while the binder and

aggregate were being mixed. Several tests were performed in this research, dynamic complex modulus, Cantabro durability, asphalt pavement analyzer, flow number, and Indirect Tensile Strength. According to this paper the optimum binder content was not affected using the 15-sec interval method. Also, the same method showed more consistency when evaluating the specific gravities of the mixtures. Basalt showed the best performance in the Cantabro loss by 2.83%. Unfortunately, this research was not able to draw significant conclusions from the rut resistance and cracking resistance.

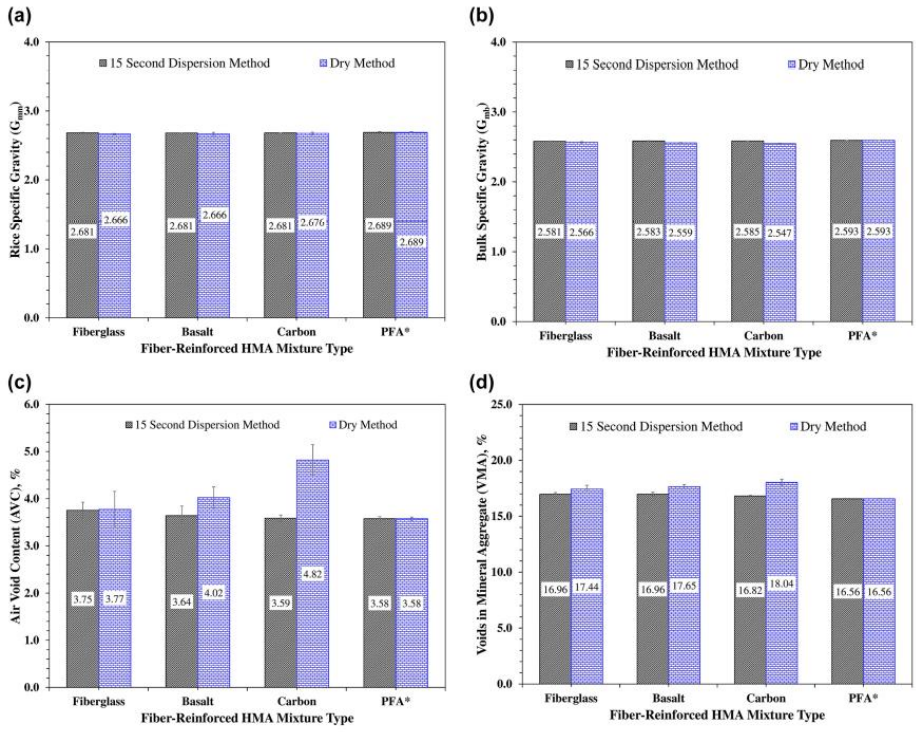

Figure 2.7: Results of the mix design for fiber-reinforced hot mix asphalt mixtures using the 15 s dispersion and dry mixing methods: (a) Rice specific gravity (Gmm), (b) bulk specific gravity (Gmb), (c) air void content (AVC), (d) voids in mineral aggregate (VMA) (Alfalah et al. 2020).

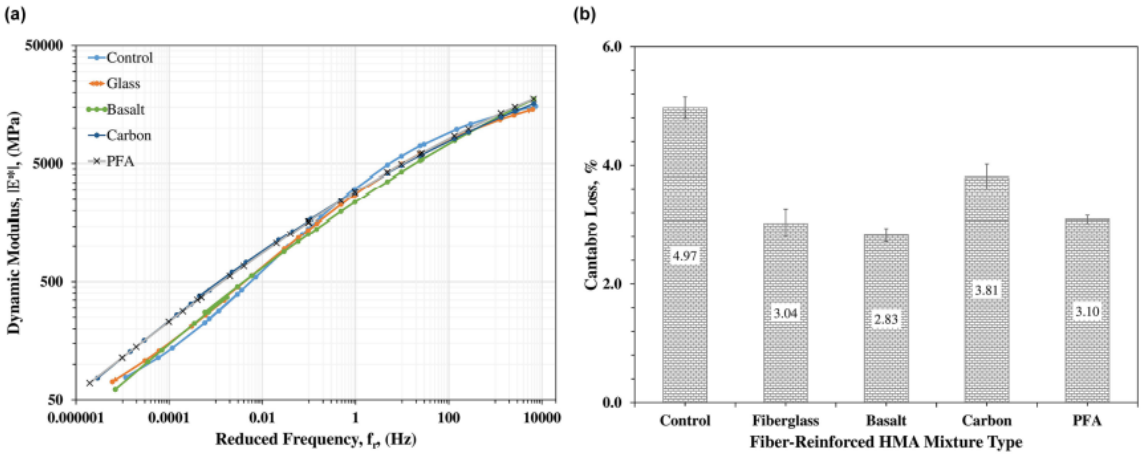

Figure 2.8: Test results for unreinforced and fiber-reinforced hot mix asphalt mixtures: (a) dynamic complex modulus, |E* |, master curves and (b) Cantabro loss (Alfalah et al. 2020).

Guo et al. (2020) evaluated the performance of asphalt with different fiber material, dimensions, and content. The main goal was to identify how these three parameters affected the performance of the material. Three "commonly" fibers were evaluated, basalt, polyester, and lignin. To assess the optimal fiber length, two types of tests were performed: the mesh-basket draindown test and the cone penetration test. In these two tests the basalt fiber length of 6mm provided the lowest mass loss in the mesh-basket draindown and the largest shear resistance in the cone penetration test. To evaluate the optimal fiber content three engineering properties were measured: high temperature stability, low temperature cracking, and water susceptibility. The research determined 0.4 wt. % to be the optimal fiber content for the previously mentioned properties. In both fiber content and fiber length, basalt fibers were determined to perform better than the polyester and lignin fibers. Figure 2.9, shows results obtained from this research, where

GFRAC, BFRAC, SFRAC were glass, basalt, and steel fibers respectively, and where the following number represents the length of the fiber in mm.

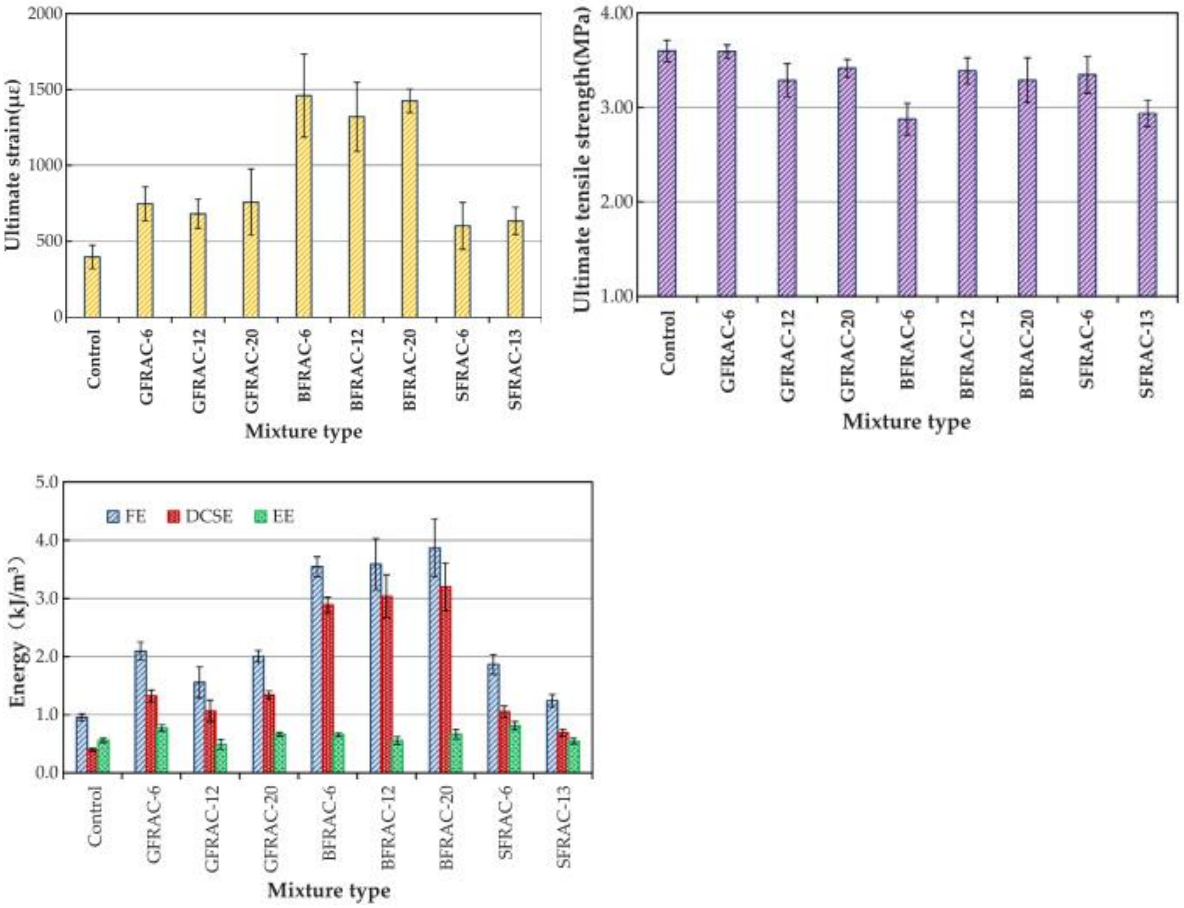

Figure 2.9: Ultimate tensile strain of distinct groups (top left), Ultimate tensile stress of different groups (top right), and Cracking energy of different FRAC mixtures (bottom) (Guo et al. 2020).

The purpose of the research by Xu et al. (2010) is to investigate the reinforcing effects and mechanisms of fibers in asphalt concrete (AC) mixtures under temperature and water effects. Four fiber types were investigated: polyester, polyacrylonitrile, lignin, and asbestos. The Fiber Reinforced AC (FRAC) underwent laboratory experiments to determine its strength, strain, and fatigue behavior. According to the results, fibers increased AC's toughness, fatigue life, and rutting resistance. The split indirect tensile strength (SITS) at a low temperature, the ultimate flexural strain, and the flexural strength and ultimate flexural strain have been improved. While lignin and asbestos fibers produce higher flexural strength and ultimate flexural strain, which may be primarily due to their greater asphalt stabilization effect, the polymer fibers have improved rutting resistance, fatigue life, and SITS more significantly than lignin and asbestos fibers. Additionally, it has been discovered that for polyester fiber, a fiber content of 0.35% by mass of the mixture yields the best performance results in terms of rutting resistance and SITS.

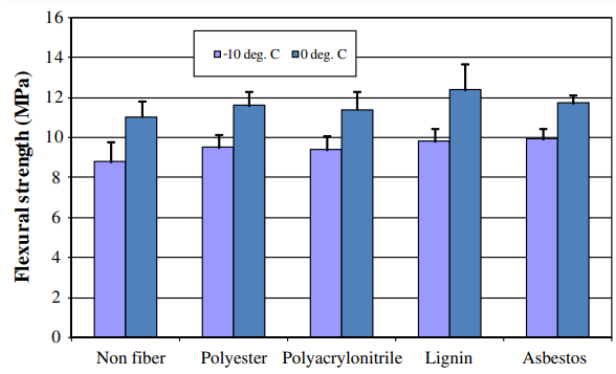

Fig. 6. Flexural strength.

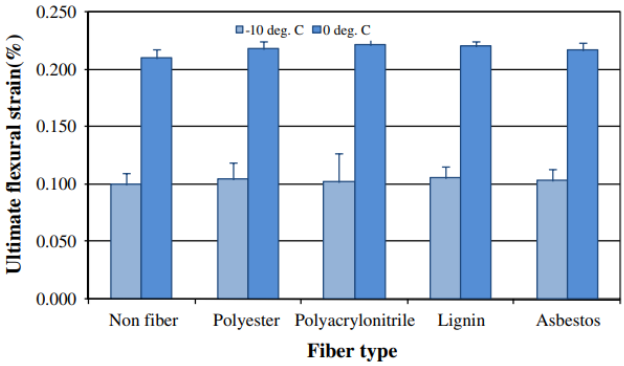

Figure 2.10: Represents the results of the Ultimate Flexural Strain of FRAC of several types of fibers (Xu et al. 2010).

Yang et al. (2016) studies the impacts of amorphous metallic fibers on several asphalt concrete (AC) attributes, including internal porosity, resistance to moisture-related damage, dynamic stability, indirect tensile strength, flexural strength, strain capacity, and toughness, will be investigated. Several AC samples with different fiber volume fractions were created and evaluated for this. Investigated were the effects of the amount of asphalt binder on the characteristics of AC with fibers. According to test results, adding amorphous metallic fibers increased the amount of air voids in AC, hence more asphalt binder was needed for AC with fibers to reach 4% air voids or less than AC without fibers. The addition of fibers reduced the

indirect tensile strength and flexural strength of AC, and the moisture-related degradation was more evident. However, the use of amorphous metallic fibers increased the dynamic stability, strain capacity at a moderate temperature, and thermal overall conductivity. Using induction heat and constraint, complete AC failure incorporating amorphous metallic fibers was successfully self-healed.

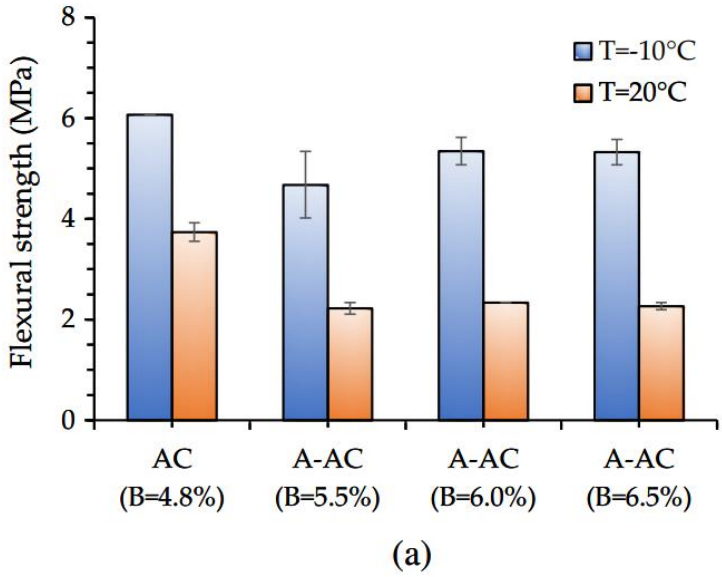

Figure 2.11: Flexural Stress vs Strain curves for several binder contents and different temperatures (Yang et al. 2016).

Mechanical Performance of FRAC

Asphalt pavements are designed to withstand the recurring loads from moving vehicles. These asphalt members under the compressive loads of vehicles still experiences split tension. This is where the fiber reinforcement is used. The use of fiber reinforcement helps improve the roadway's durability and overall lifespan (Takaikaew et al. 2017). Fiber reinforced asphalt

concrete is usually validated through material testing that can simulate standard and difficult roadway conditions (Yuanxun et al. 2014). These difficult roadway conditions are considered at high and low temperatures (Gu et al. 2022 and Gao et al. 2021) and even under special applications (Stempihar et al. 2012). Under freezing temperatures, it is very likely that the AC will undergo cracking. Under low temperatures, asphalt binder tends to stiffen, resulting in cracking. Under high temperatures, it is very likely that AC will undergo rutting. When exposed to high temperatures, asphalt binder becomes more malleable and begins to lose strength. Guo et al. (2020) studies the effects of three different fibers to observe their ability improve the material's cracking resistance. The paper determined that FRAC presented a superior Cracking energy and dissipated creep strain energy. This study also stated the fibers were able to delay the fracture process. There has been an abundance of research done in the use of fibers in asphalt to mitigate the effects of low (Jenq et al. 1993; Ziari et al. 2020; and Motamedi et al. 2020) and high (Behbahani et al. 2009 and Zhang et al. 2018) temperatures. Additionally, fibers have proven to improve the composite material's shear strength (Miao et al. 2019), fatigue performance (Wang et al. 2018), and self-healing (Liu et al. 2017). There are many ways that the performance of AC can be improved by fibers, however this study will focus on select categories.

Guo (2014) evaluates the impact of steel fibers in asphalt on road performance. The author tested the high temperature stability of samples with different fiber contents. He also measured the bending strength and the bending tensile strength under a range of temperatures. This range of temperature went from -40ºC to 10ºC. These samples were also prepared under a variety of fiber contents from 0% to 3%, however the percentage of either weight of volume was

not specified. With the bending test the author measured the bending tensile strength in “high” temperatures and the crack resistance in low temperatures.

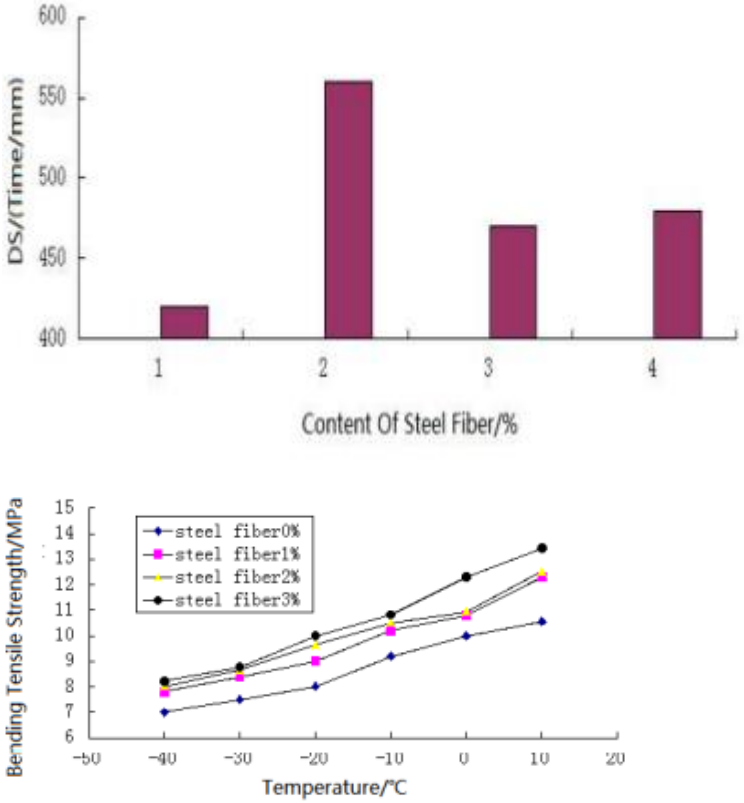

Figure 2.12: Influence of steel fiber content on the stability (top) and bending tensile strength of asphalt concrete under different temperature, different content of steel (bottom) (Guo 2014).

Liu et al. (2021) examined steel fibers in asphalt concrete. Although the main goal was to measure induction heating, different fiber lengths and content were measured in a variety of engineering performances. This research evaluated the steel fiber reinforced asphalt through high-temperature rutting resistance, low-temperature cracking resistance, and freeze-thaw cycles resistance. This experiment proved that FRA showed improvement in all the tests. Also, induction heating was shown to be more effective by increasing the length of the fibers. Figure 3.13 shows the performance of steel fibers with different lengths, where heating rate (HR),

thermal conductivity (TC), maximum bending strain (MBS), tensile strength ratio (TSR), and dynamic stability (DS) is measured and compared.

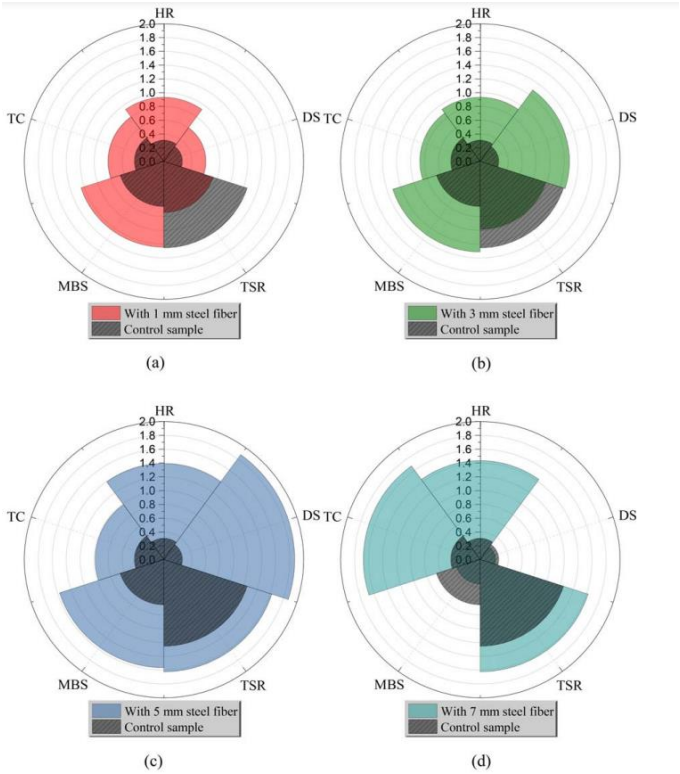

Figure 2.13: The radar charts for five types of asphalt mixture (Liu et al. 2021).

Park et al (2015) conducted Indirect Tensile Tests at -20ºC on fiber reinforced asphalt to examine the reinforcement provided by steel fibers. Specimens with Carbon fibers, Polyvinyl alcohol fibers, and control were also developed in this experiment. The tests conducted in this experiment evaluated the cracking resistance, indirect tensile strength, Cracking energy, and post-cracking energy. Low temperature cracking was proven to be mitigated by the addition of steel fibers. Fiber dimensions, deformations, and content had a major impact on the performance of the asphalt.

Noorvand et al. (2018) analyzes rutting and fatigue in the fiber reinforced asphalt. These asphalt specimens were reinforced with the Aramid synthetic fiber. To measure the performance, Dynamic modulus, repeated load permanent deformation, and uniaxial fatigue tests are performed. There were 3 different kinds of samples that were tested in this experiment: Control, "Overall good dispersion of synthetic fiber (FA)", and Poor dispersion of the fiber (FB). Overall, this research saw an improvement by the FA by 130% in the flow number test, while the control and the FB had similar results. Fatigue was overall improved by fibers compared to control. The author later concluded that the orientation of the fibers played a major role in the results. The paper claims that fatigue and permanent deformation depended on the testing configuration compared to the fiber orientation.

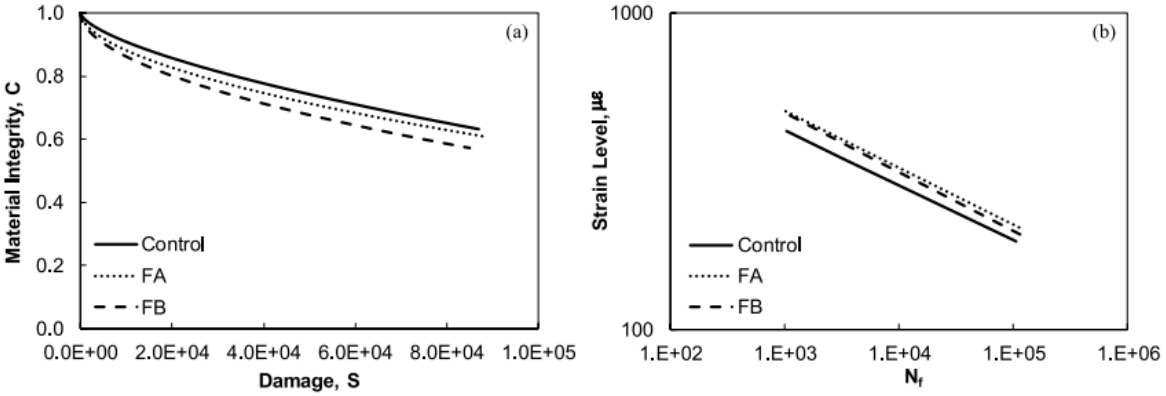

Figure 2.14: Accumulated strain during flow number test (Noorvand et al. 2018).

Lou et al. (2021) studies fiber additive, gradation type, nominal maximum aggregate size (NMAS) (Figure 2.15), and asphalt types. The author claimed that those are only a few of the variables that could have an impact on the characteristics of asphalt mixtures. Ten different types of asphalt mixtures were created to assess how these elements affected the crack resistance of the mixture. To evaluate the test samples' resistance to cracking, the indirect tensile asphalt cracking test (IDEAL-CT) and semicircle bending test (SCB) were used. To determine the correlation

between various characteristics, the parameters of the results of these two tests were also employed. A scanning electron microscope (SEM) test was also used to examine the asphalt mixture's microcracks. The findings suggested adding basalt fiber could further improve the asphalt mixture's capacity to resist cracking. In comparison to Superpave (SUP) asphalt mixtures, Stone Matrix Asphalt (SMA) demonstrated superior anti-cracking performance. The ability of asphalt mixtures to resist cracking may be reduced by an increase in the nominal maximum particle size.

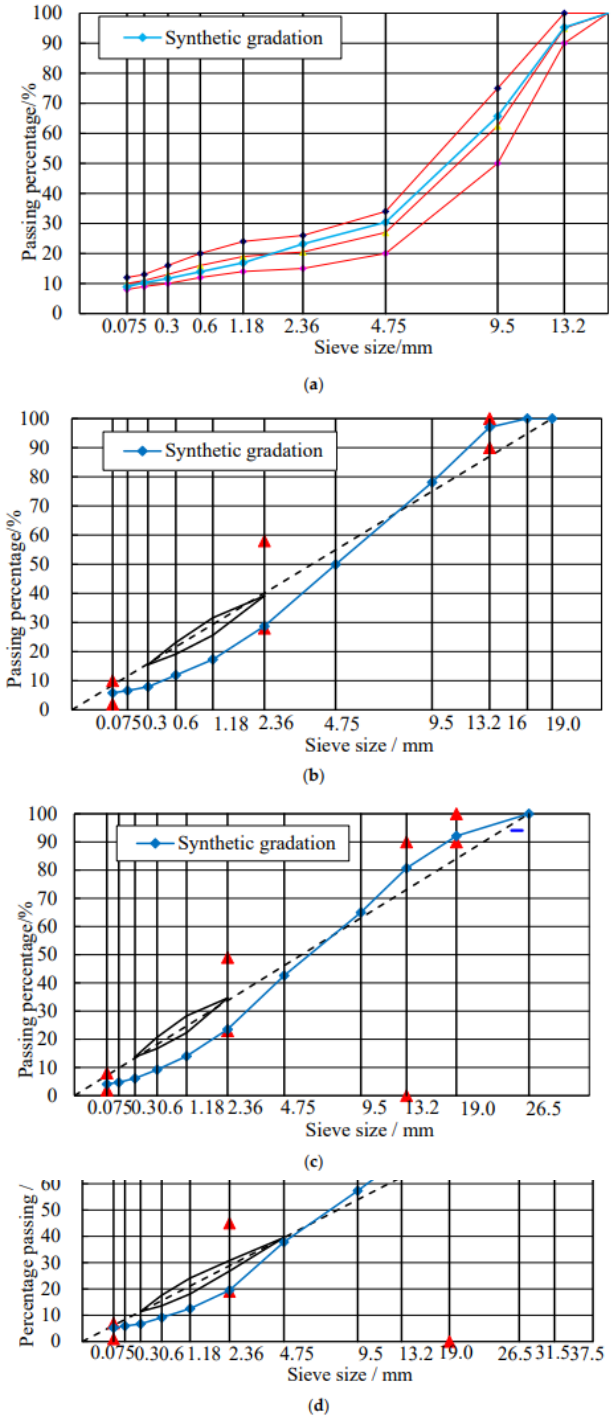

Figure 2.15: Gradation curves for SMA-13 (a), SUP-13 (b), SUP-20 (c), SUP-25 (d). (Lou et al. 2021)

CHAPTER III

EXPERIMENTAL PREPARATIONS

This research will attempt to determine the effects of fiber-aggregate interlocking. A literature review exploring previous work analyzing the effects of fiber-aggregate interlocking must be analyzed. Also, a literature review concerning the use of Fiber reinforced asphalt concrete and its performance compared to other conventional methods. An analysis of different types of fibers and their impact on the performance of the material. A method to test the fiber-aggregate interlocking must be determined. To accomplish this, materials must be acquired, aggregate gradation and binder specifications must be determined, and a test that can allow the observation of the impact of the fiber-aggregate interlocking must be made.

Material Acquisition

Two types of densely packed asphalt mixtures must be determined to test the impact of interlocking mechanism. Stone Matrix Asphalt (SMA) and Dense Graded (DG) asphalt will be mixed with fibers. Test samples will contain 0.5%, 1.0%, and 1.5% fibers by volume. Three types of fibers will be tested using dense graded, these fibers include thin steel hooked fibers, thick steel fibers, and Polyvinyl Alcohol (PVA). The PVA and the smaller steel fibers share similar dimensions, PVA's diameter and length are approximately 0.65mm and 30mm respectively. While the hooked steel fibers having a diameter and length of approximately

0.60mm and 30mm. The larger hooked steel fibers have a diameter of 0.95mm and a length of 39mm. Additionally, control specimens will be developed. As previously mentioned, these samples will be tested under 3 different temperatures. These temperatures are for now: -20ºC, 20ºC and 40ºC. This will allow us to observe the interlocking mechanism under different asphalt conditions. However, to determine the optimum binder content, a group of 12 samples of SMA and Dense Graded samples will be developed respectively. Finally, to determine the effectiveness of the interlocking mechanism a compressive test will be conducted. This will place the material under shear stress allowing us to measure the interlocking of the asphalt and aggregate.

As previously stated, two types of asphalt mixtures are made: Dense Graded (DGA) and Stone Matrix Asphalt (SMA). Both types are composed of the same materials, however their gradations curve are drastically different. Most aggregates were supplied by a local supplier VMK materials**,** shows the location and available materials used. The coarse aggregate supplied was a blue limestone Figure 3.1, while the finer aggregate was pulverized river rock Figure 3.2. As seen in Figure 3.3**,** the two mixtures gradations are very distinct from each other. Dense Graded is also known as Well Graded because the size of rocks needed fill as much of the asphalt with a large variation of finer particles and a smaller quantity and percentage of course aggregate. The DG curve is seen to be even, proving the balance of finer to course. Because of this type of gradation, the fine aggregate can fill most of the voids between the courser aggregate, this type of compact grading allows the asphalt to rely less on the weaker binder and more on the compact set of particles. The fibers used in this experiment were previously purchased from several different companies. Figure 3.4 shows an image of the three different fibers used in this experiment.

Figure 3.1: Blue limestone used for the research.

Figure 3.2: Pulverized sand used for the research.

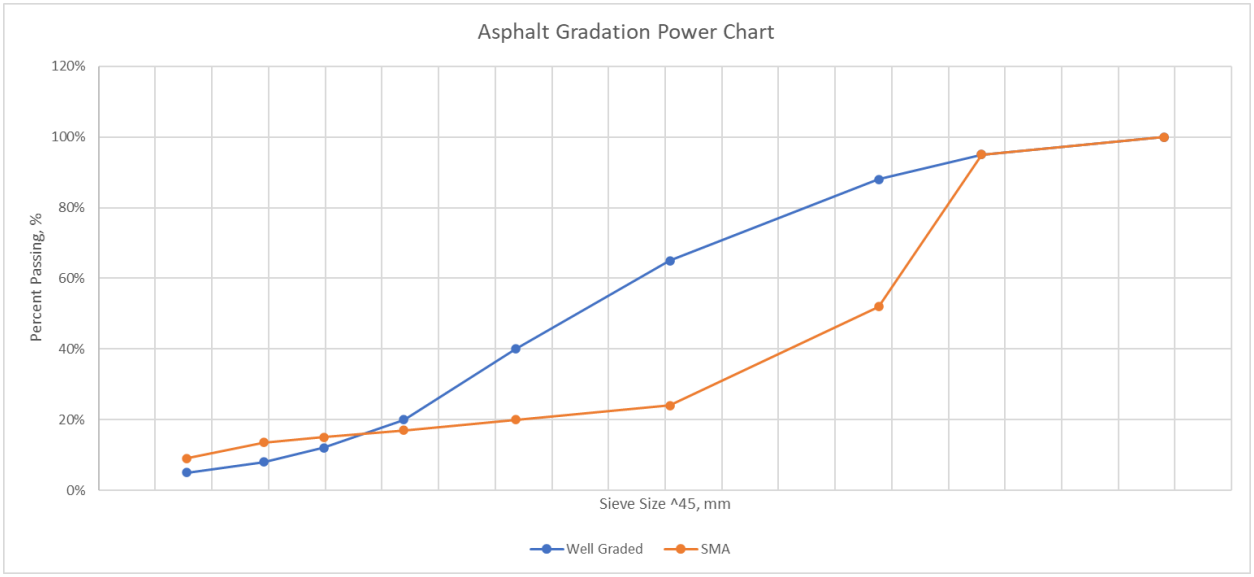

Figure 3.3: Asphalt Aggregate Gradation curve.

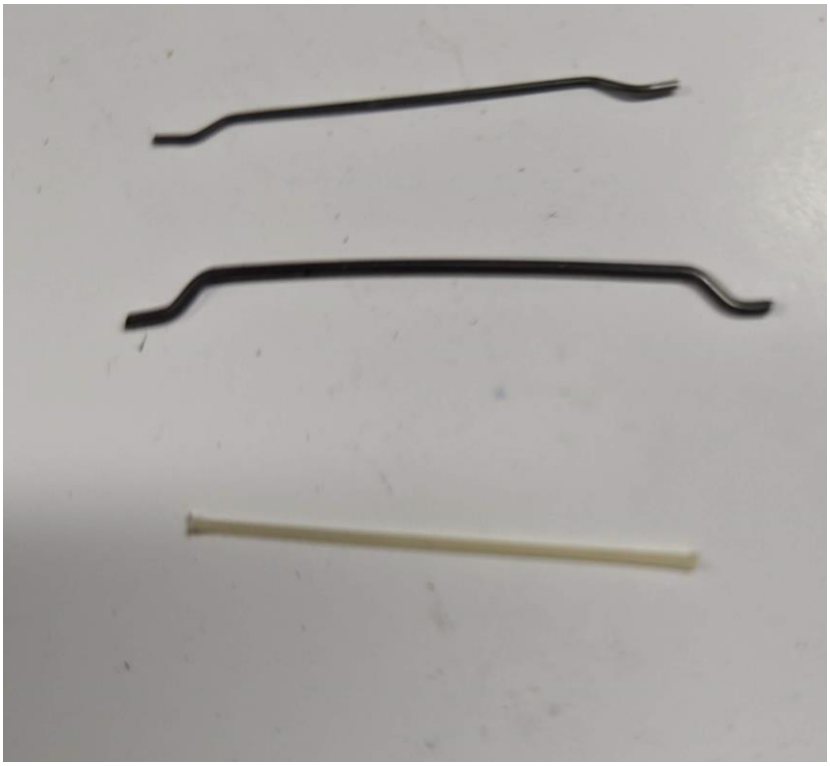

Figure 3.4: Fibers used in this experiment. Smaller, hooked steel fiber (top); larger, hooked steel fiber (middle); PVA fiber (bottom).

The use of Stone Matrix relies on another philosophy or another form of thinking, unlike DGA, SMA relies less on filling gaps between the larger particles (aggregate). The idea behind SMA was to rely more on the larger aggregate using stone-to-stone contact to interlock. However, because of the lack of the smaller particles, voids between the larger aggregate must be filled with more asphalt binder. As previously stated, asphalt binder is not a very strong material, and must be limited as much as possible. Too much binder is also harmful to the long-term performance of asphalt and can cause extensive rutting. Finally, the asphalt was donated by the local office of the Valero Energy Corporation. Because of the extreme warm weather in Texas, the Performance Grade 77ºC -22ºC (PG 77-22) asphalt binder was selected. This asphalt

binder was meant to encompass the extreme heats and barely cold temperatures that are experienced in this state.

AASHTO Standards

AASTHTO T83 Maximum Theoretical Specific Gravity or Gmm is used to determine the maximum compacted state of an uncompacted and loose asphalt mixture. This means that the aggregates and the binder have been mixed, but not compacted. This method was a key value to determine the air voids of both DGA and SMA. All equipment was properly calibrated prior to conducting the tests to assure consistency across all tests. In this experiment a balance (electronic scale) that is precise to the 0.1g, volumetric metal container Figure 3.5 with at least the capacity of 1000ml with the appropriate connections to the pump Figure 3.6, a vacuum pump able to pull until 30.0mm Hg of absolute pressure continuously for 15 min. Figure 3.7, Auto-Rice Controller that can actively show the active pressure Figure 3.8, and a water bath were prepared for this experiment Figure 3.9.

Loose asphalt was collected and separated manually to small pieces no larger than a quarter inch and was allowed to cool to room temperature. A recording of the weight of the metal container (volumetric flask) was taken before beginning the experiment. The sample was placed in the metal container and filled with enough water to cover the sample. All floating particles were manually sunk. After, a special lid was placed over the container and the special connection was connected to the pump (see Figure 3.10 for the entire setup). The pump was turned on removing entrapped air by creating negative air pressure. The pressure was maintained at 27.5 +- 2.5 mm Hg for 15 minutes. Additionally, the volumetric flask was placed on a vibrating machine

assisting in the release of entrapped air. Once all air was removed the volumetric flask was again filled, and the weight was recorded.

Figure 3.5: Metallic volumetric flask.

Figure 3.6: Appropriate connections from volumetric container to pump.

Figure 3.7: Air pump.

Figure 3.8: Electronic auto-rice controller.

Figure 3.9: Water bath equipment setup.

Figure 3.10: Air void removal Equipment setup.

AASHTO T166 Bulk Specific Gravity or Gmb is a procedure that is also done to determine air voids in compacted asphalt mixtures. In this experiment a scale with the same specifications as the one used for the AASHTO T83 experiment, a Suspension apparatus is used, a water bath for immersing specimens, a damp towel which means that the towel is wet and is not excreting any excess water when tightened, and an oven is used. See Figure 2.9 for full water bath setup, where the scale used in this experiment has a hook underneath to measure the weight of the submerged specimens.

The specimen was briefly placed in the oven and allowed to cool before measuring its weight. The water bath was allowed to overflow and the water to stabilize. The balanced was set to zero and the damp dowel was prepared. The specimen was then placed in the suspension apparatus for 4 +- 1 minutes. The weight was recorded of the submerged specimen. After the specimen was removed from the water bath and the excess water was quickly removed by the damp towel. The weight of the sample under Saturated Surface Dry (SSD) was recorded.

AASTHO T68 Determination of Volumetric Properties in Asphalt Laboratory Compacted Specimens is the procedure used for determining the volumetric properties, most noticeably percent air voids and voids in mineral aggregate (VMA) of laboratory compacted asphalt specimens. As previously mentioned, this procedure is dependent on AASHTO's T83 and T166. The results obtained from the last two experiments have given us Theoretical Maximum and Bulk Specific Gravity. The equations used to determine percent air voids is listed below. Equation 2.1 is the formula used to determine Bulk Specific Gravity, Equation 2.2 is the formula used to obtain Maximum Theoretical Specific Gravity, and finally Equation 2.3 is used to determine percent air voids.

Bulk Specific Gravity = A / (B -C)

Where,

A = mass (g) of specimen in air

B = mass (g) of specimen SSD in air

C = mass (g) of specimen in water

Equation 2.1: Bulk Specific Gravity for Asphalt Samples (Gmb).

Maximum Theoretical Specific Gravity = C / (C-F)

Where,

C = mass (g) of sample

F = mass (g) of sample submerged in water

Equation 2.2: Maximum Theoretical Specific Gravity for Asphalt Samples (Gmm).

% Air Voids = (1 – D / E) * 100

Where:

D = Bulk Specific Gravity

E = Maximum Specific Gravity

Equation 2.3: Percent Air Voids for Asphalt Samples using Gmb and Gmm.

AASHTO T84 Effective Specific Gravity for Fine Aggregate procedure is done to determine the apparent specific gravity of fine aggregates in addition to the bulk and bulk SSD specific gravity, and the absorption of fine aggregates after being submerged in water. In this procedure a balance with a precision up to 0.1g was used, a glass pycnometer with a capacity of at least 1000ml, a cone shape metal mold with an opening of at least 40 +- 3 mm on top and an opening of at least 90+-3 mm opening at the bottom, a metallic tamper with a weight of 340 +- 15 g with a flat circular tamping face with a diameter of 25 +- 3 mm. Figure 3.11 shows the metallic cone and tamper.

Figure 3.11: Metallic Cone and Tamper.

The preparation of the fine particles is as follows: the sample of fine aggregates was sieved to make sure that all the sample passed the #4 sieve. The sample was submerged in water for at least 15 hours, following that the excess water was removed, and the wet fine particles were placed in an oven to allow to heat to the required consistency of the SSD sample. Once the sample reached what is believed to be SSD conditions, a cone test was performed. The metallic cone was placed over a flat non-absorbent surface and filled up completely with the SSD fine particles. The metallic tamper was dropped 25 times over the fine sample from a height approximating 5mm. Any excess was cleared from the mold and the metallic cone was lifted vertically. If the material slumped “slightly” meaning that it has approximated SSD conditions. If the material did not slump, the sample was placed for a few minutes in the oven and the

procedure was repeated, if the sample did not hold its shape, additional water was added and placed again in the oven, after the procedure was repeated.

Once the material is prepared, the procedure can proceed. 500 +- 10g of SSD fine material is prepared and the mass recorded. The pycnometer is partially filled, and the SSD material is introduced into the water Figure 3.12. The pycnometer is filled with approximately 90% of water. The pycnometer is rolled, inverted, and agitated for 15 to 20 minutes. This is done to remove any air bubbles entrapped in the fine aggregate. The pycnometer is calibrated by filling to the calibration mark with water, with any foam or water removed with a paper towel. The pycnometer is completely dried, and the mass is recorded. The material is removed from the pycnometer and collected in a pan or bowl. Any remaining aggregate is washed out from the pycnometer into the bowl. The specimen is placed in the oven over night and allowed to cool to room temperature before recording the weight. Equation 2.4 show the calculations done to determine the desired specific gravities.

Figure 3.12: Pycnometer with a capacity of 1000ml.

Apparent Specific Gravity (Gsa) = A / (B + A – C)

Where,

A = mass (g) of dry sample

B = mass (g) of pycnometer filled with water

C = mass (g) of pycnometer, sample, and water

Equation 2.4: Apparent (Effective) Specific gravity of Fine Aggregate.

AASHTO's T85 Effective Specific Gravity for Coarse Aggregate is a procedure do not to determine the specific gravity and absorption of course aggregate. The bulk specific gravity, Saturated Surface Dry (SSD), and/or apparent specific gravities can be obtained from this procedure. The coarse aggregate in this procedure is consisted of all aggregate that was retained by the #4 sieve. The materials needed for this procedure are a scale with at least a 5kg capacity with the accuracy of at least 0.1g, a sample container such as a wire mesh basket with a capacity of 1 to 2 gal to contain the coarse aggregate with a nominal maximum size of 37.5 mm (1 ½ inch), a water tank large enough to submerge the basket with an overflow valve to ensure that the water level is kept consistent, a suspension apparatus to hold the wire mesh basket in place while submerged, and a larger absorbent towel.

To prepare the sample, the coarse aggregate is prepared under the same conditions as it were prepared for an asphalt specimen. All materials that were not retained by the #4 sieve are rejected from this procedure. The aggregate is thoroughly washed to remove any smaller particles attached to the larger aggregate. The test sample wis then dried and allowed to cool at room temperature. Once the preparations were done, the coarse aggregate was submerged in water for 15 to 19 hours. The wire mesh basket is placed inside the water bath, filled until overflow, and allowed to stabilize. Excess water was drained from the bowl that was containing the coarse aggregate. The aggregate was then taken out and dried with an absorbent cloth. The aggregate was still wet, however there was not excess water around it. The aggregate was allowed to rest in a bowl with a wet towel over them. Through this method the SSD condition was met and maintained. The weight of the SSD aggregate was recorded. The aggregate was then transferred in the wire mesh basket and submerged using a twisting motion. The water level in the water bath was allowed to stabilize and the submerged weight of the aggregate was then

recorded. The aggregate was then transferred into a dry bowl and dried in the oven over night. The aggregate was then cooled to room temperature and the weight of the dry aggregate was recorded. Equation 2.5 were used to determine necessary properties of the aggregate.

Apparent Specific Gravity (Gsa) = A / (A- C)

Where,

A = mass (g) of dry specimen

B = SSD mass (g)

C = weight (g) in water

Equation 2.5: Apparent (Effective) Specific Gravity of Course aggregate.

AASHTO T312 Gyratory Compactor is used for the compacted samples of the asphalt concrete are used to determine the volumetric and mechanical characteristics of the mixture. The volumetric and mechanical properties are then used to determine the best mix design or control of the mixture during real world applications. The goal of the gyratory compactor is to simulate the density, orientation of aggregates, and structural characteristics of asphalt pavements in real-world applications. In addition, analysis of the compacted specimens can be used to evaluate densification properties, moisture sensitivity, quality control, and in this scenario to test the use of fibers in asphalt concrete.

Gyratory Compactor used in this experiment is shown in Figure 3.13**.** The compactor is equipped with a dial that measures, records, and stores information from the compacted specimen. This information can include the number of compactions, height, gyration angle, force

of compaction, and other number of inputs needed to compact the specimens and to ensure quality of compaction. The mold used in this experiment is shown in Figure 3.14**.** This mold is 7.5 mm thick, 250 mm tall, and an inside diameter of 150 mm. The Steel used was hardened to at least a Rockwell Hardness of C 48, meaning that it can withstand the weight of the material, the force exerted by the compactor, and the internal pressure crated by the compaction. The force exerted was approximately 600 KPa per compaction, with a total number of compactions of 100 per specimen (as recommended by the Federal Highway Administration for a ESAL of 3 to 30 million vehicles), this number was used with all specimens unless specified otherwise. The internal angle of 1.16º +- 0.02º was used as recommended by AASHTO T 312.

Figure 3.13: Gilson Co. Superpave Gyratory Compactor.

Figure 3.14: Asphalt Compaction Mold.

The Gyratory compactor was calibrated and issued maintenance as needed. Additional support was given by the manufacturers and any change in internal maintenance was done with their careful recommendation and detailed specifications.

For using the Gyratory Compactor and preparing the asphalt samples, the correct aggregate needs to be prepared, the proper amount of binder needs to be determined, a total amount of batch mixture (fine aggregates, coarse aggregates, and binder) approximately 6200 g (to achieve the target height of 150mm) had to be prepared. The binder is then heated to 160 ºC to achieve the consistency required to heat up the PG 70-22 and for mixing the aggregates. This ensures that the binder fluid has the correct consistency to coat all the aggregates. The

ingredients are then mixed and placed inside the mold. The mold is then placed inside the Gyratory Compactor and a lid is placed over the mold. This allows the compactor to apply pressure from the bottom of the mold and have an equal reaction from the top. Once the machine completes the number of gyrations, the lid is lifted, and the asphalt specimen is extruded from the top.

Preparations and Asphalt Mixing

Extensive preparations are needed to properly compact the specimens. This includes sieving and washing, temperature and moisture control, asphalt mixing, and asphalt content determination. Steps taken to ensure the quality required to mix are detailed below. Unlike the previous methods, these actions were taken upon recommendation from the advisor of this project who has experience mixing and previously determined this to be the most effective way to ensure proper specimen preparation.

Unlike concrete, aggregates are not bough prepared, they are prepared to ensure the best quality possible. As previously stated, blue limestone was used for the coarse aggregate, while pulverized river rock was used as fine aggregate. The materials were purchased locally, specified sizes were not possible to purchase, however size ranges had to be determined and then purchased to satisfy the range needed for the DG and SMA. Once the materials were safely and cautiously delivered to our lab, the aggregates were separated by mechanical sieving equipment (Figure 3.15). The aggregates were previously separated to satisfy the requirements of DG and SMA, these sizes were: 1/2”, 3/8”, #4, #8, #16, #30, #50, #200, and Pan size. Sieves used in this experiment are U.S.A. Standard Testing Sieves, following ASTM E-11 Specifications. The pan

size particles that were used was limestone powder, these are filler particles that can pass through the #200 sieve, this was a separately purchases product from a hardware store. Once the particles were separated into different sizes, they would have to be washed. Washing the aggregate was a method of quality control, each rock contained dust around them, this dust can be considered fine particles added to the mixture and would through off the ratio between fine and coarse particles. Because of this, the aggregates needed to be washed to remove a significant portion of the smaller particles attached.

Figure 3.15: Mechanical Sieve Shakers.

As a result of the washing, the particles used would absorb moisture, and it would through off the required weight needed for the selected aggregate. As another form of quality control, we began to remove the moisture through extreme heat. Washed aggregates would be

left overnight before they were weighted and mixed. Through moisture control, we also included temperature control. Temperature control was not a method used for quality assurance, a necessity needed to properly mix the binder with the aggregates and fiber. Using the available oven, the binder needed to be heated up to 160 ºC to ensure proper consistency, when mixing, everything had to be approximately that temperature and maintained to that temperature. The oven used was calibrated to ensure safety measures would be taken if any accident would have occurred. The oven utilized was old, and the previous owners did not ensure proper safety or any maintenance that the oven needed. If the temperature dropped, the asphalt would not mix properly, and the results would have been determinantal. The aggregates, mixing paddle, bucket, spoons, spatulas, pans, casting molds, and everything that would eventually encounter the aggregate had to be maintained at a certain temperature. Unfortunately, temperature and moisture control created a significant bottleneck in the output of asphalt samples. Because everything had to be left overnight or at least 4 to 6 hours, mixtures could not be created every day. In addition, the oven used had a limited capacity. When heating asphalt binder, additional precautions were taken to ensure the quality would be maintained. Unlike the other materials, the binder can only be placed in the oven for certain number of hours and a limited number of applications. The binder would be placed 2 hours prior to mixing to ensure that oxidation would not occur. This is a chemical reaction that happens when a substance encounters oxygen or any oxidizing substances. Asphalt binder is extremely vulnerable to this especially when it reaches the temperatures needed to mix. As precaution, the binder would remain in a seal container (Figure 3.16) preventing as much oxygen from encountering it. In addition, any asphalt mixtures were also limited to reuse because of this.

Figure 3.16: Metallic asphalt containers.

Before the asphalt samples that were eventually used for the experiment were mixed, the binder contents were determined. As previously stated, the specimens were to be created with the dimensions of 150 x 150 mm (diameter and length), 100 gyrations, and a target goal of 4.0 percent air voids. With these constraints, the required amount of asphalt binder needed to be determined. A percent binder content of 4.37% and 5.5% by weight was used for the Dense Graded and Stone Matrix Asphalt samples, respectively. Each of these specimens would be tested using AASHTO standards, and whichever had the correct air voids was used for the remainder of the experiment.

Once the correct measurements of ingredients were obtained, the mixing would begin. First, all the aggregates would be placed inside the bucket, then the aggregate was mixed under dry conditions (no binder). During this step fibers were “sprinkled” into the mixture to ensure proper mixing. This method allowed for a more thorough mix and ensured proper distribution of fibers and avoided the creating of clumps. The aggregate and paddle were allowed to heat up once more before adding the binder. Once this was completed, binder would be added to the

mixture and thoroughly mixed using our asphalt mixer **(see** Figure 3.17). Once thorough mixing was achieved, the asphalt mixture would be place in the oven again, but in aluminum trays**.** The mixture would be taken out and placed into molds in quantities of 6200 g per sample. Paper disks were placed below and above the sample to protect the compactor from the binder. After this the mold was placed into the gyratory compactor where it would be completed.

Figure 3.17: Asphalt mixing apparatus.

Additionally, safety is an important aspect of mixing asphalt. Because of the temperature that was required to mix, the lab was an "outside" lab, open to the local hot and humid temperatures. Special precautions were taken to ensure the safety of the individuals mixing. Safety equipment used were insulated gloves, long sleeve lab coats, closed toed shoes, and pants. The temperature of the metallic equipment meant that it was dangerous to handle any equipment

without the proper safety. In addition, because of the proximity to the oven and the extreme temperatures outside, extra precautions were taken to stay hydrated and to stay cool. Breaks had to be taken frequently to avoid any heat related incidents. Fans were purchased to cool the room as well.

Loading Equipment

This experiment utilized the Material Testing System (MTS) machine to perform monotonic compression tests. This machine is best test the presented hypothesis, by forcing stone-to-stone contact through compression and allowing us to evaluate the impact of fibers within the asphalt's skeletal system. The system needed to be able to withstand the force needed to force structural failure within the specimen, while recording 3 important parameters. These parameters included Force, Displacement, and Time. From those parameters displacement was the controlling factor. The machine was set to displace 1 mm/min. The data obtained from the MTS was a .csv file displaying a constant displacement and how much force was needed to continue displacing at the given rate. Figure 3.18 shows the machine used in this experiment.

Additionally, tests were conducted under Cold, Room Temperature, and Hot conditions. The specimens were placed in a freezer and an oven overnight to ensure that the specimen is the same temperature. Tests were conducted quickly, one at a time.

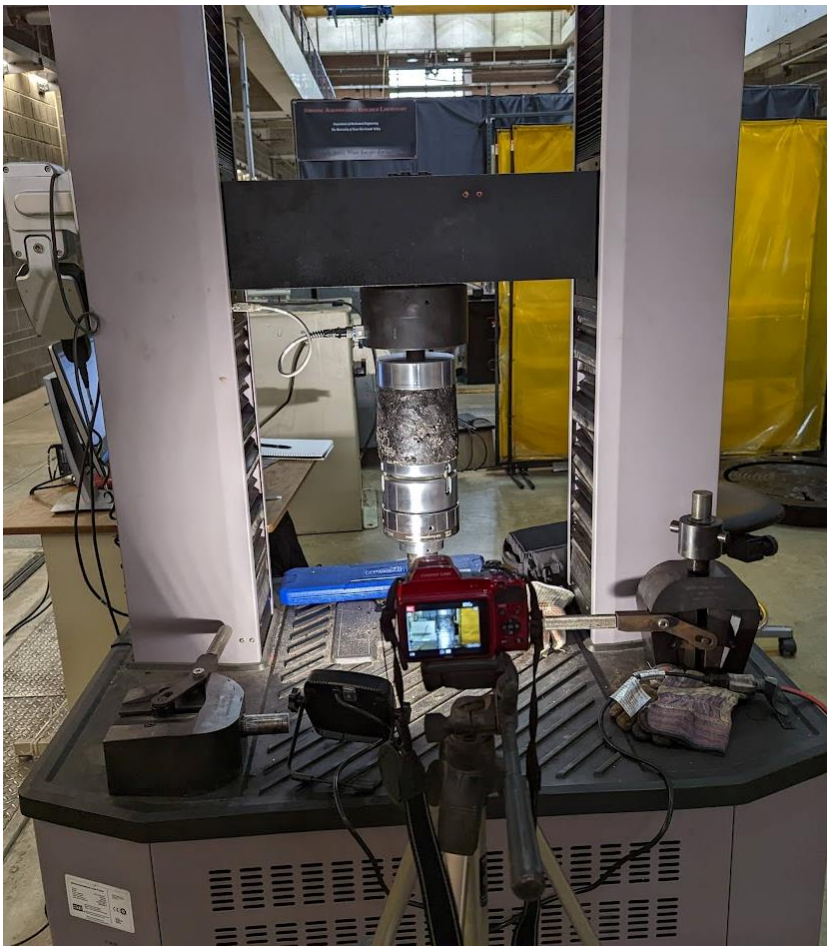

Figure 3.18: MTS Machine.

CHAPTER IV

RESULTS AND DISCUSSION

The results from this experiment will present the data that was collected from the material preparations and the data obtained from the MTS equipment. The information is provided to interpret the impact that the fibers had on the asphalt. Data showing the average air void content for each of the fiber material and percentage will be demonstrated. A set of stress-strain curves will be presented to evaluate and compare the impact that the fiber type and percentage has on the materials performance. A table depicting the Fracture and Post-Cracking energy of each sample will be displayed. Figures comparing the Fracture and Post-Cracking energy to the control asphalt specimens will be shown. Finally, tables comparing the performance of individual specimens will be show.

Test Results

The data presented will be shown in terms of the asphalt gradation (DG or SMA) fiber type (H, L, and PVA) and fiber percent (05, 10, or 15). H represents the smaller hooked steel fibers, while L represents the larger hooked steel fibers, PVA is the polyvinyl alcohol. PVA was made using Dense Graded (DG) exclusively, so there was no initial specification. Additionally, SMA was tested using the smaller hooked fibers exclusively, meaning that there is no fiber specification. DGL05 refers to the Dese Graded Large hooked steel fibers at a 0.5 percent fiber

by volume. PVA10 is the Dense Graded asphalt using 1.0 precent fiber by volume. SMA15 is the Stone Matrix Asphalt using the small Hooked steel fibers utilizing 1.5 percent fiber by volume.

As previously mentioned, tests were conducted under 3 drastically different temperatures. The tests are done using the small, hooked steel fibers using DG and SMA. In Figures 4.12 and 4.13 the C is for Cold, R for Room Temp, and H for Hot. The rest of the labels follows the same labeling than as previously mentioned.

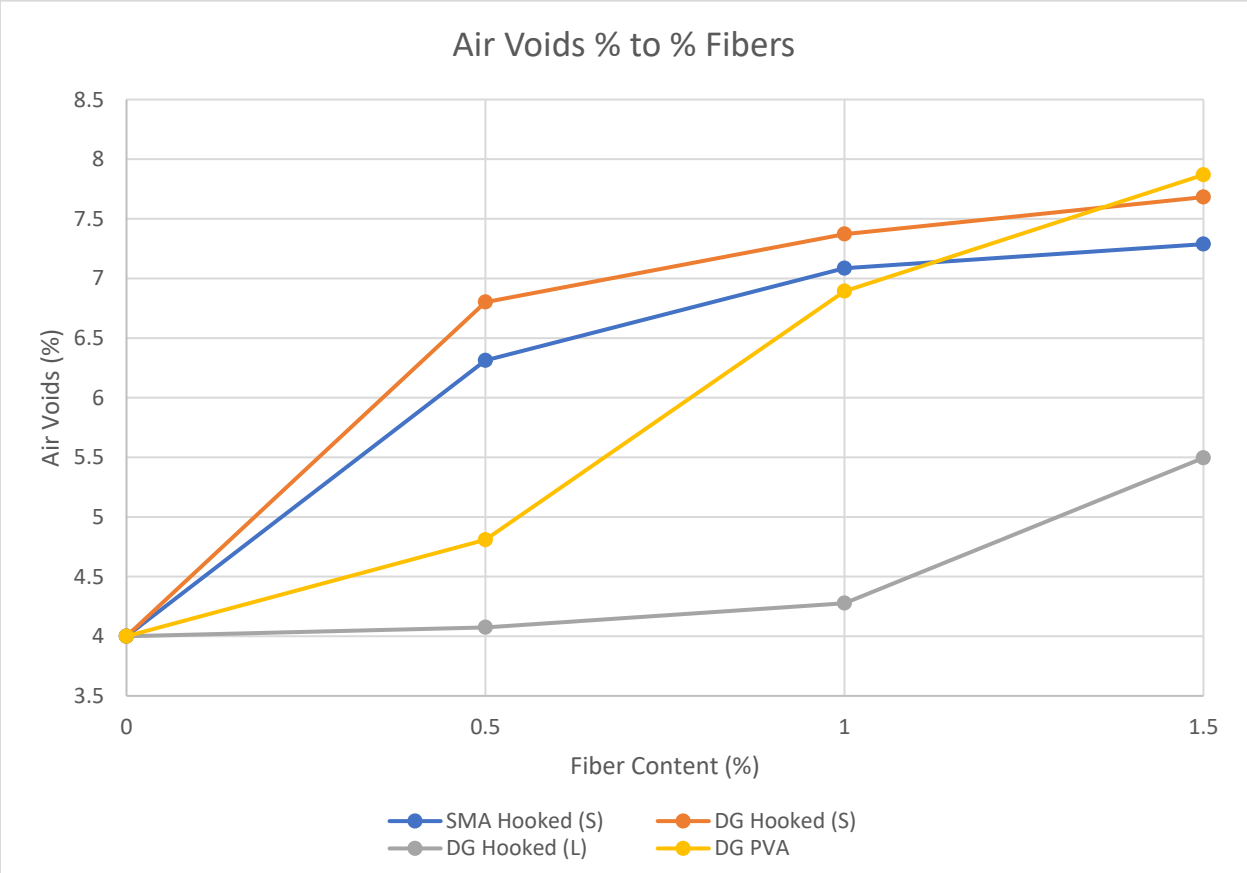

Figure 4.1: Air Voids to Fiber Percentages

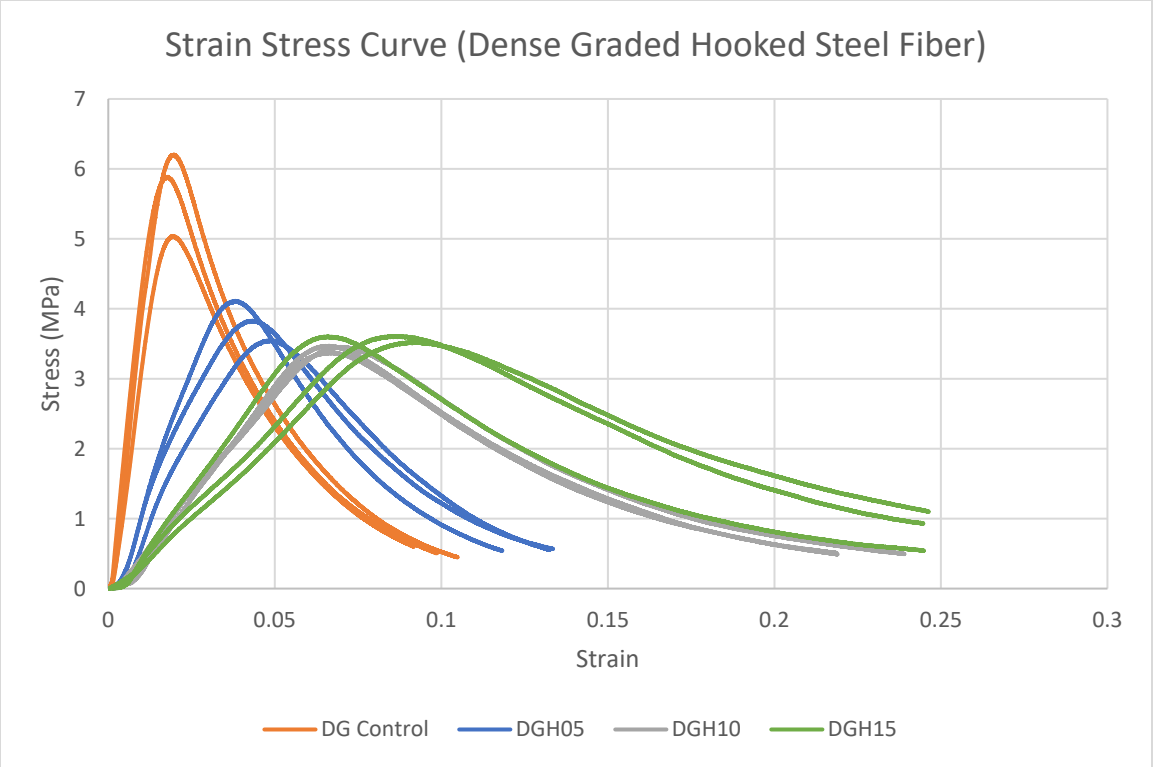

Figure 4.2: Stress Strain Curve for DG Hooked Steel Fibers.

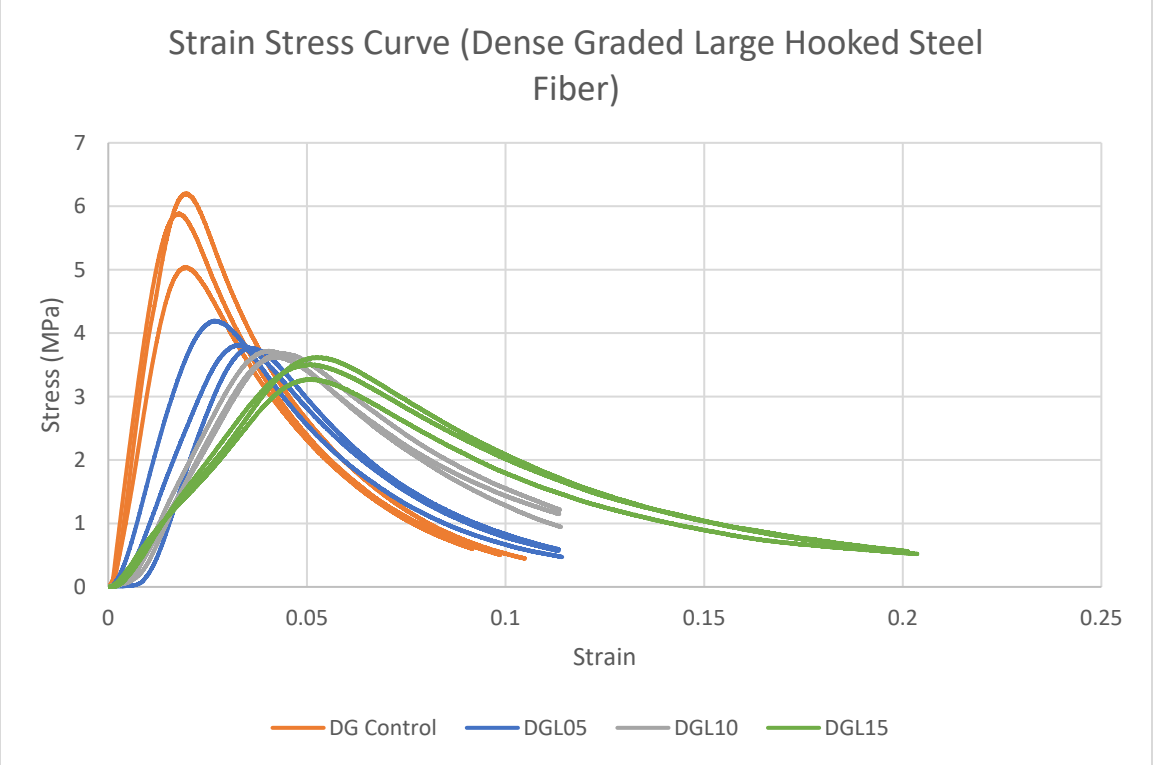

Figure 4.3: Stress Strain Curve for DG Large Hooked steel Fibers.

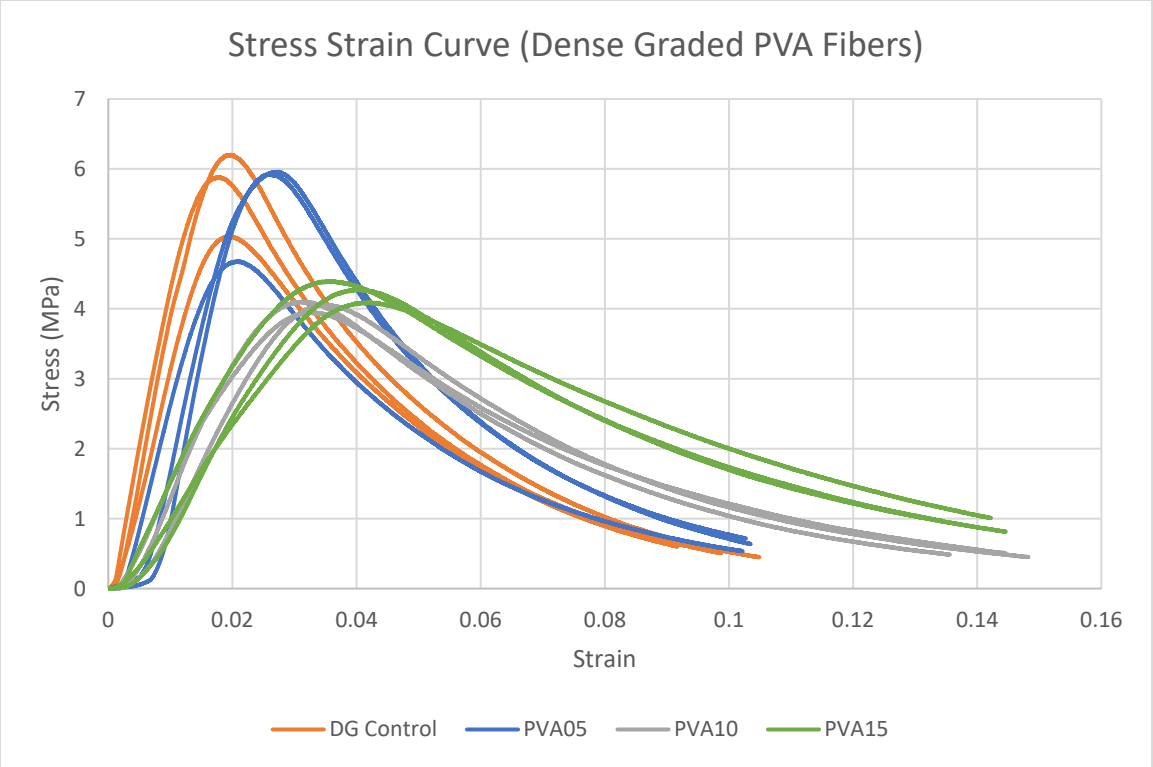

Figure 4.4: Stress Strain Curve for DG PVA Fibers.

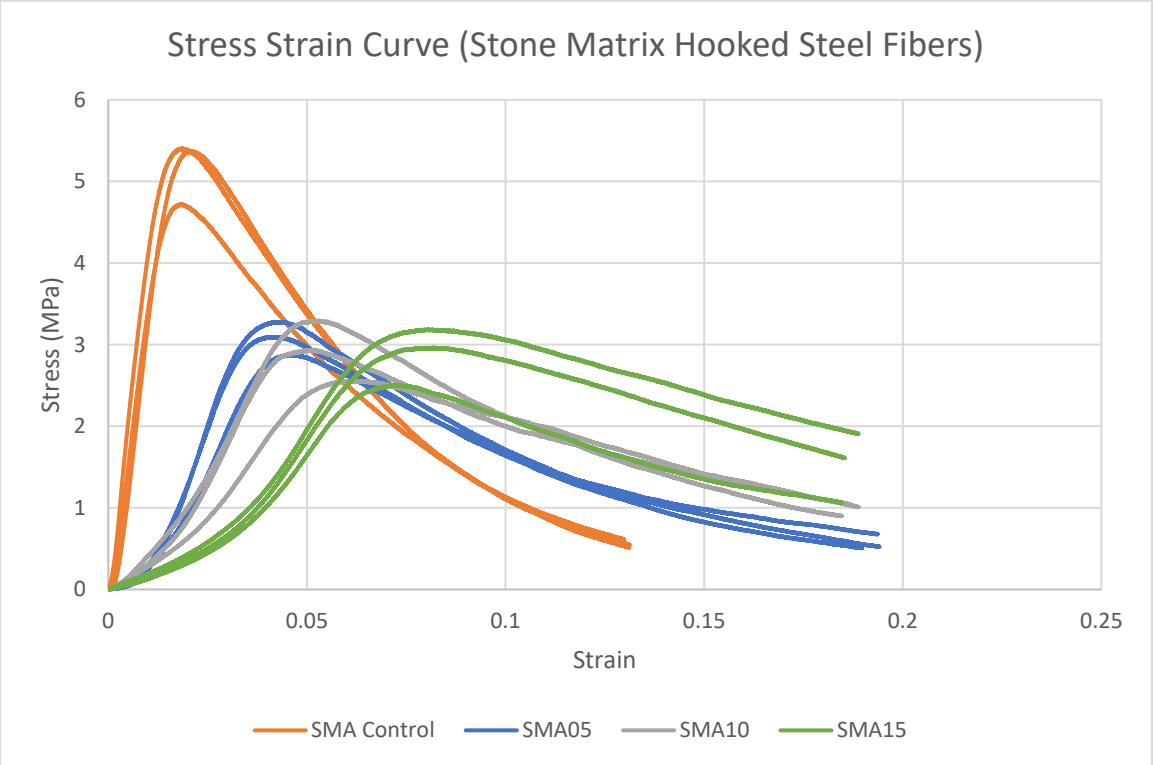

Figure 4.5: Stress Strain Curve for SMA Hooked Steel Fibers.

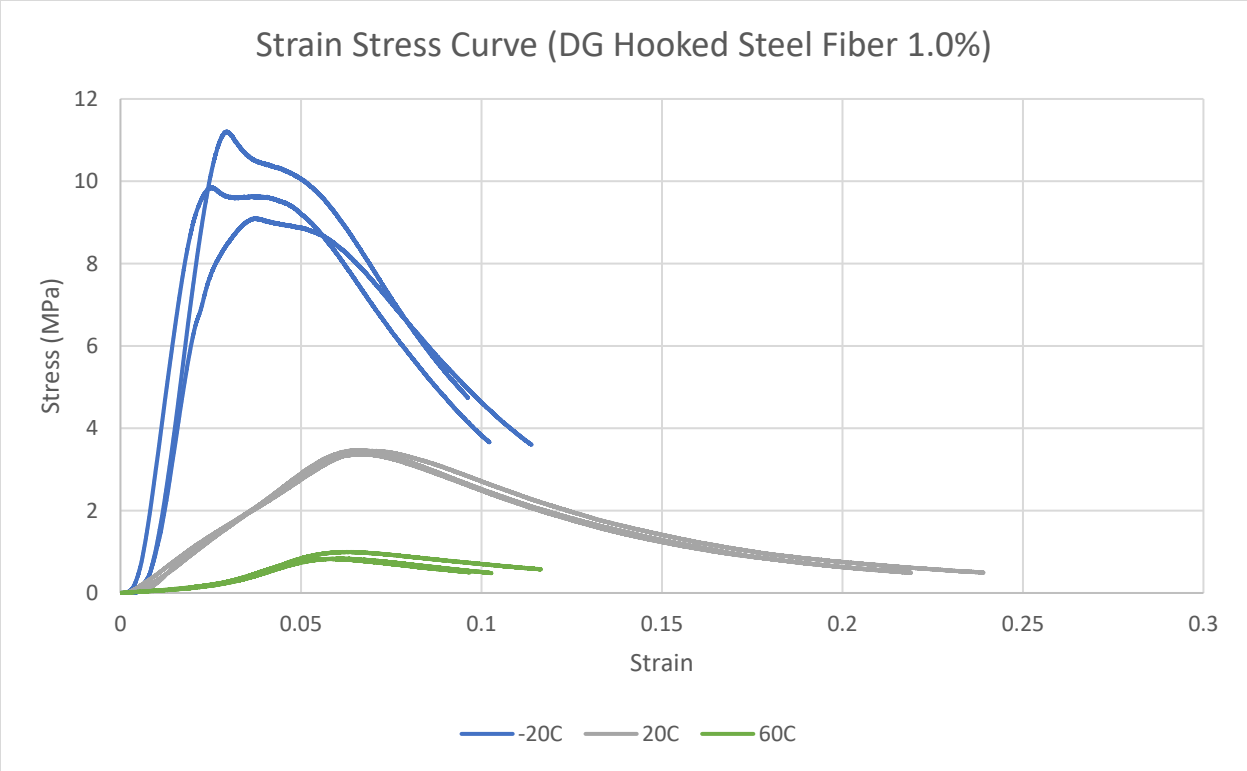

Figure 4.6: Stress Strain Curve for DG under different Temperatures,

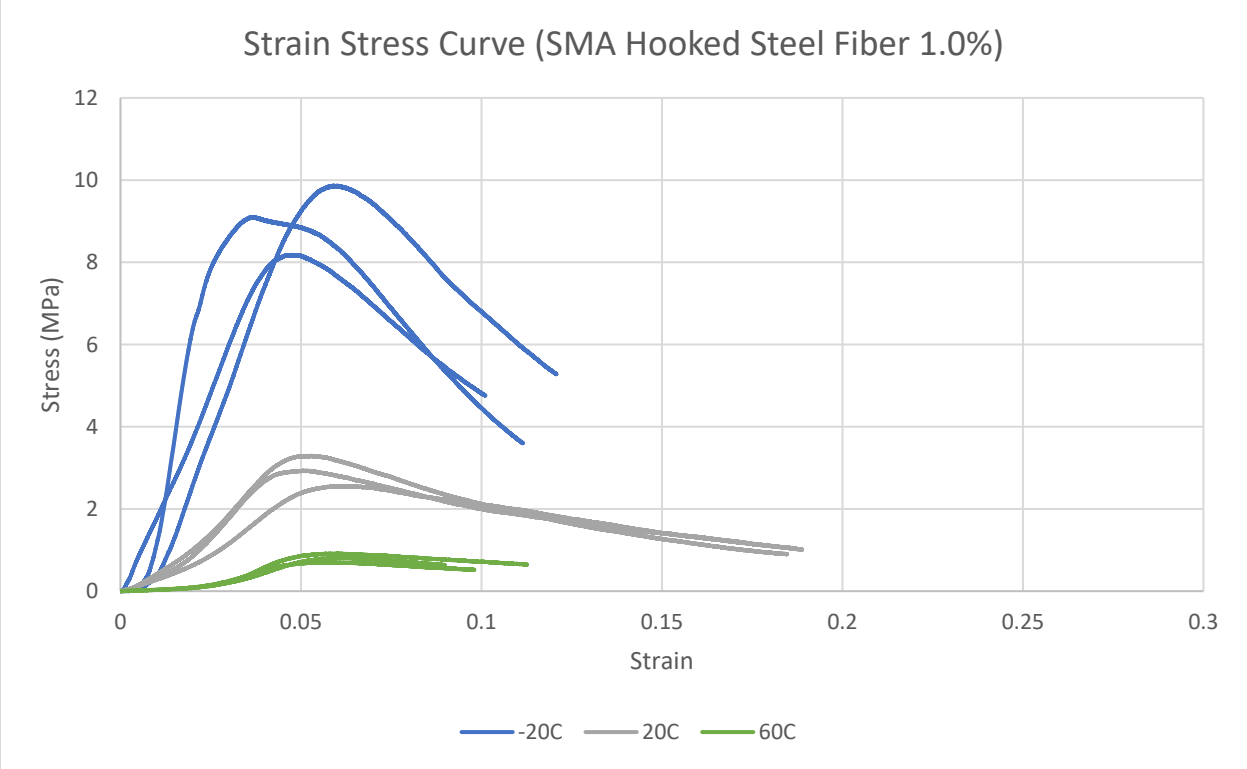

Figure 4.7: Stress Strain Curve for SMA under different Temperatures,

Table 4.1: Key values obtained from each specimen. (Peak Stress (σ_p), Stress at PE (σ_f), FE and PE in MPa. Peak strain (ε_p))

Specimen	σ_p	ε_p	σ_f	$2\sigma_p$	FE	PE	%Air
DGH05 1	3.54600	0.04765	1.49500	0.09530	0.09170	0.12320	7.585025635
DGH05 2	3.81150	0.04464	1.58000	0.08928	0.10050	0.11972	6.599578574
DGH05 3	4.11300	0.03805	1.77700	0.07610	0.08450	0.11324	6.220780595
DGH10 1	3.45300	0.68500	1.67200	1.37000	0.23800	0.17960	7.482155373
DGH10 2	3.37200	0.06700	1.55000	0.13400	0.22500	0.16670	7.513291511
DGH10 3	3.46600	0.06580	1.65600	0.13160	0.11670	0.16700	7.119710125
DGH15 1	3.59900	0.06700	1.76700	0.13400	0.29400	0.18100	7.898019796
DGH15 2	3.60900	0.08754	1.81100	0.17508	0.17520	0.24260	7.533926537
DGH15 3	3.51810	0.09200	1.83200	0.18400	0.17530	0.25150	7.613894265
DGL05 1	4.19430	0.02703	2.29400	0.05406	0.06206	0.09000	3.943898667
DGL05 2	3.74400	0.03762	1.55340	0.07524	0.06537	0.09734	3.961885724
DGL05 3	3.81100	0.03365	1.83460	0.06730	0.06680	0.09494	4.41780984
DGL10 1	3.65300	0.04682	1.73280	0.09364	0.09300	0.12370	4.221767632
DGL10 2	3.62200	0.04247	1.37634	0.08494	0.07657	0.11523	4.228179261
DGL10 3	3.69600	0.03830	2.18500	0.07660	0.06864	0.11585	4.38103533
DGL15 1	3.25900	0.05307	1.64400	0.10614	0.09880	0.12970	5.509877295
DGL15 2	3.61780	0.05370	1.86800	0.10740	0.10604	0.14780	5.701642557
DGL15 3	3.48750	0.05350	1.83200	0.10700	0.10749	0.14200	5.274253835
PVA05 1	4.67618	0.02103	2.74167	0.04206	0.05377	0.08065	4.629087741
PVA05 2	5.95604	0.02684	2.88027	0.05369	0.07956	0.11861	4.877803235
PVA05 3	5.90729	0.02539	3.09364	0.05077	0.06408	0.11609	4.920557026
PVA10 1	3.94845	0.03304	2.29810	0.06607	0.07654	0.10462	7.193900664
PVA10 2	4.09912	0.03089	2.08192	0.06177	0.06847	0.11758	6.619022105
PVA10 3	4.05800	0.03554	2.15410	0.07109	0.07571	0.11111	6.865019371
PVA15 1	4.08122	0.04013	2.66572	0.08026	0.08873	0.13891	8.610788122
PVA15 2	4.36148	0.03873	2.51301	0.07746	0.10559	0.13322	7.409367171
PVA15 3	4.27516	0.04066	2.34414	0.08133	0.09322	0.13585	7.585740008
SMA05 1	2.86353	0.04856	1.72261	0.09712	0.06931	0.11170	6.592786456
SMA05 2	3.09049	0.04049	2.09903	0.08097	0.05842	0.10769	6.277831009
SMA05 3	3.27248	0.04305	2.06154	0.08610	0.06790	0.11616	6.067878834
SMA10 1	2.93410	0.05161	1.94891	0.10321	0.07557	0.12633	7.269612032
SMA10 2	3.23735	0.05809	1.79893	0.11618	0.10372	0.14298	6.882681985
SMA10 3	2.54843	0.06484	1.69807	0.12968	0.08813	0.13861	7.104444075
SMA15 1	3.18841	0.08067	2.23728	0.16134	0.12140	0.22295	7.333341064
SMA15 2	2.49730	0.07081	1.45780	0.14161	0.07416	0.14158	7.071572272
SMA15 3	2.95673	0.08380	1.84772	0.16760	0.12150	0.20463	7.457659496
DG Control 1	5.03987	0.01939	3.19898	0.03879	0.05436	0.08127	4
DG Control 2	6.19720	0.02011	3.50562	0.04022	0.07093	0.09557	4
DG Control 3	5.88581	0.01798	3.64648	0.03596	0.06290	0.08614	4
SMA Control 1	5.38807	0.01994	4.08220	0.03988	0.07023	0.09549	4
SMA Control 2	5.36593	0.02149	3.92304	0.04299	0.06741	0.10149	4
SMA Control 3	4.72369	0.01838	3.74670	0.03676	0.05168	0.07891	4

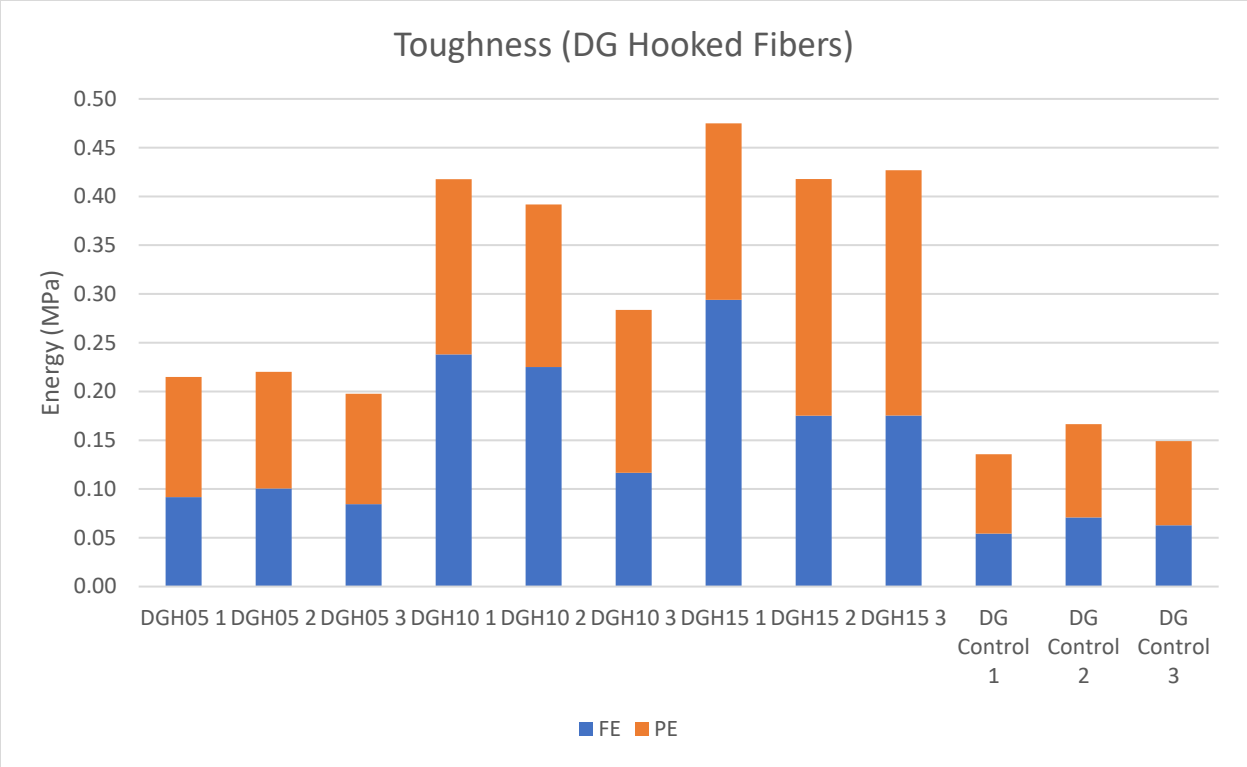

Figure 4.8: Toughness of DG Hooked Steel Fibers.

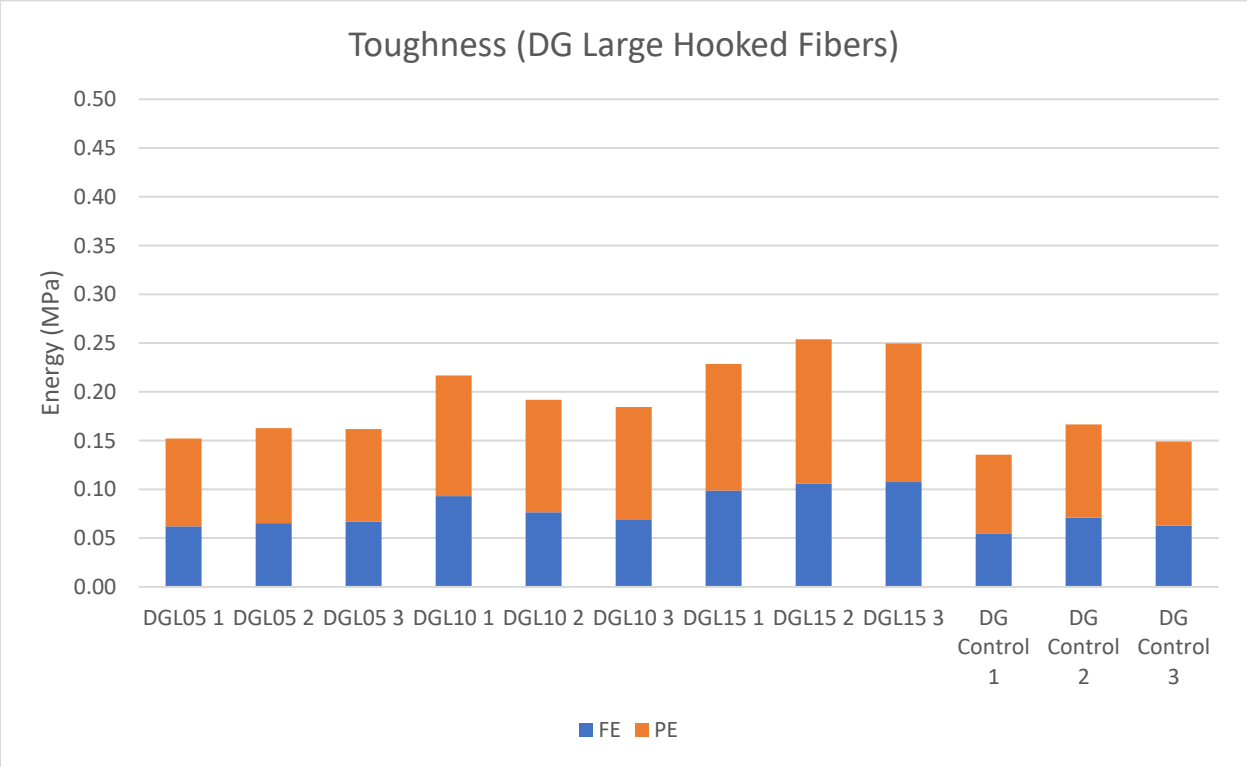

Figure 4.9: Toughness of DG Large Hooked Steel Fibers.

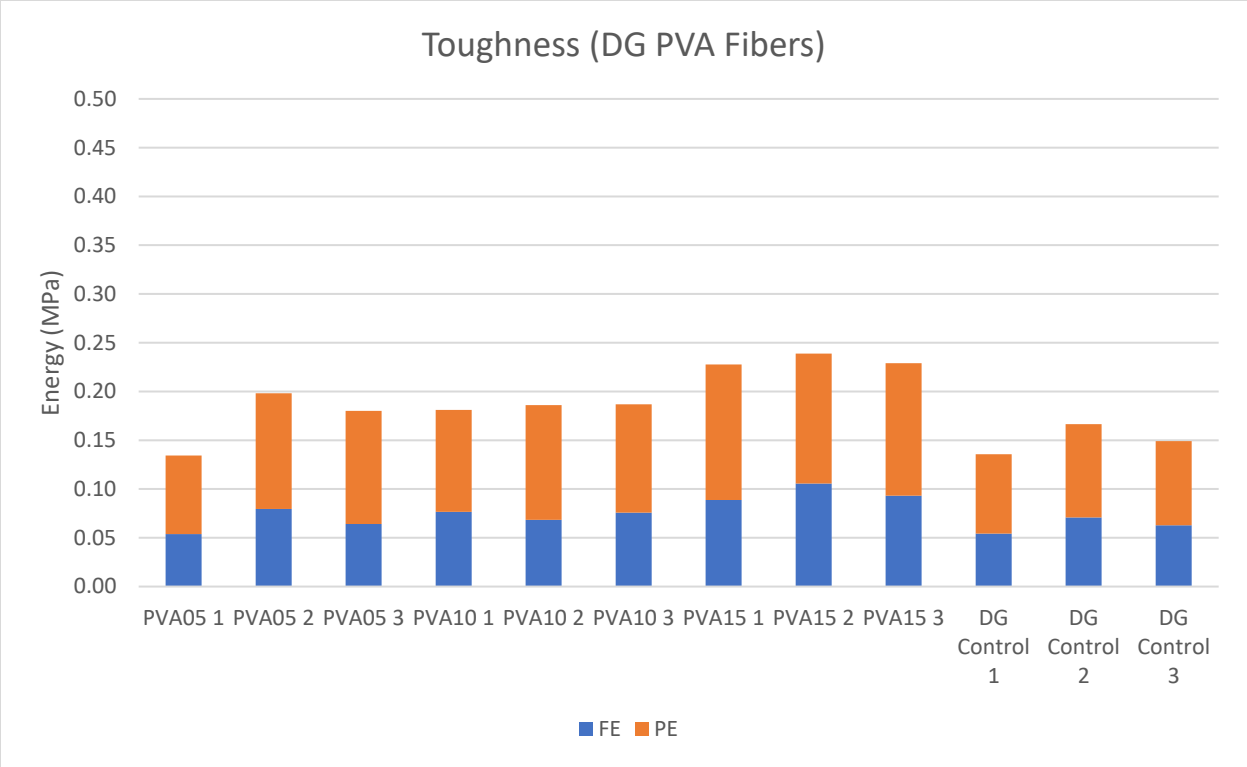

Figure 4.10: Toughness of DG PVA Fibers.

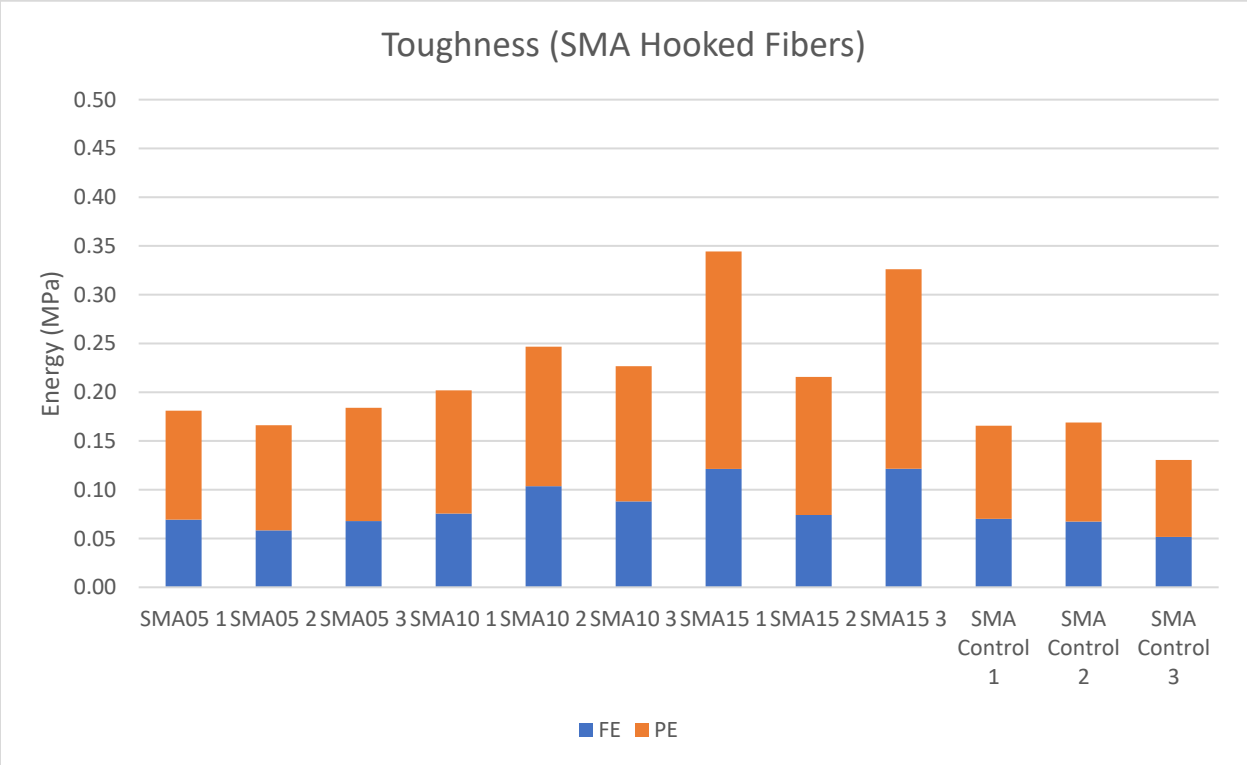

Figure 4.11: Toughness of SMA Hooked Steel Fibers.

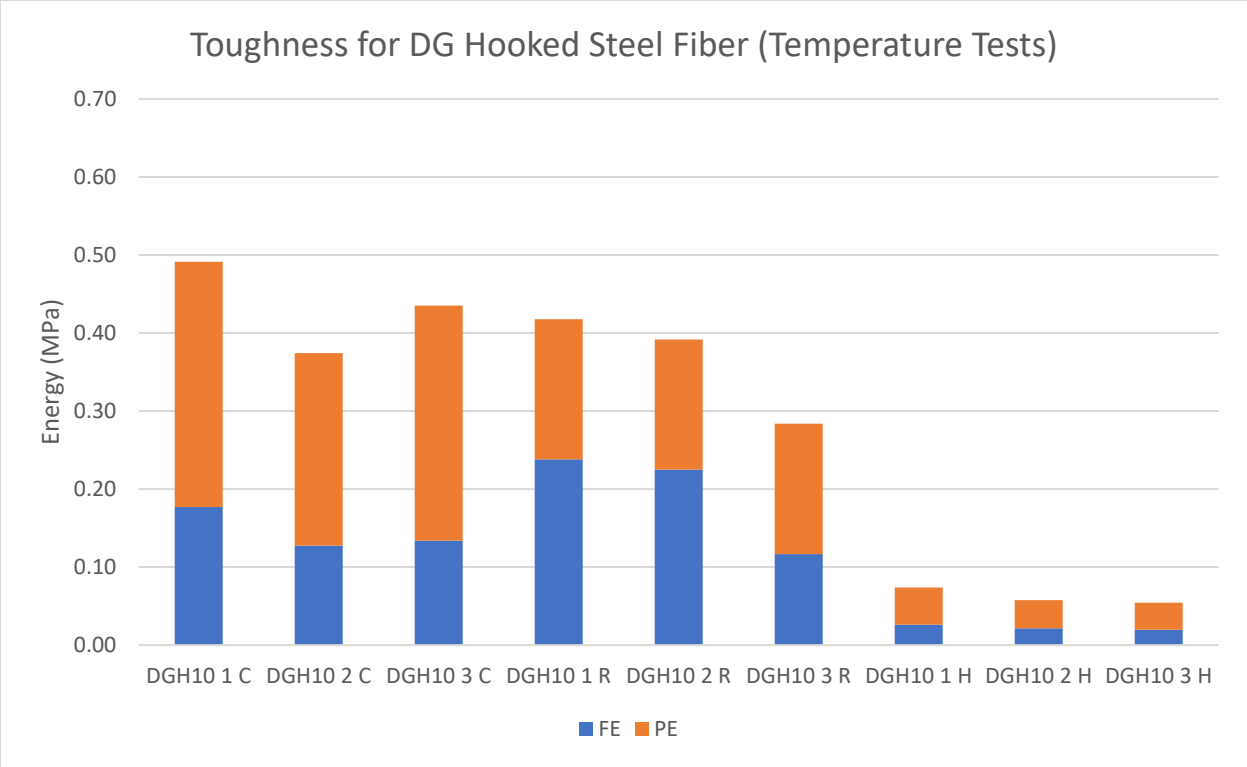

Figure 4.12: Toughness of DG FRAC under different temperatures.

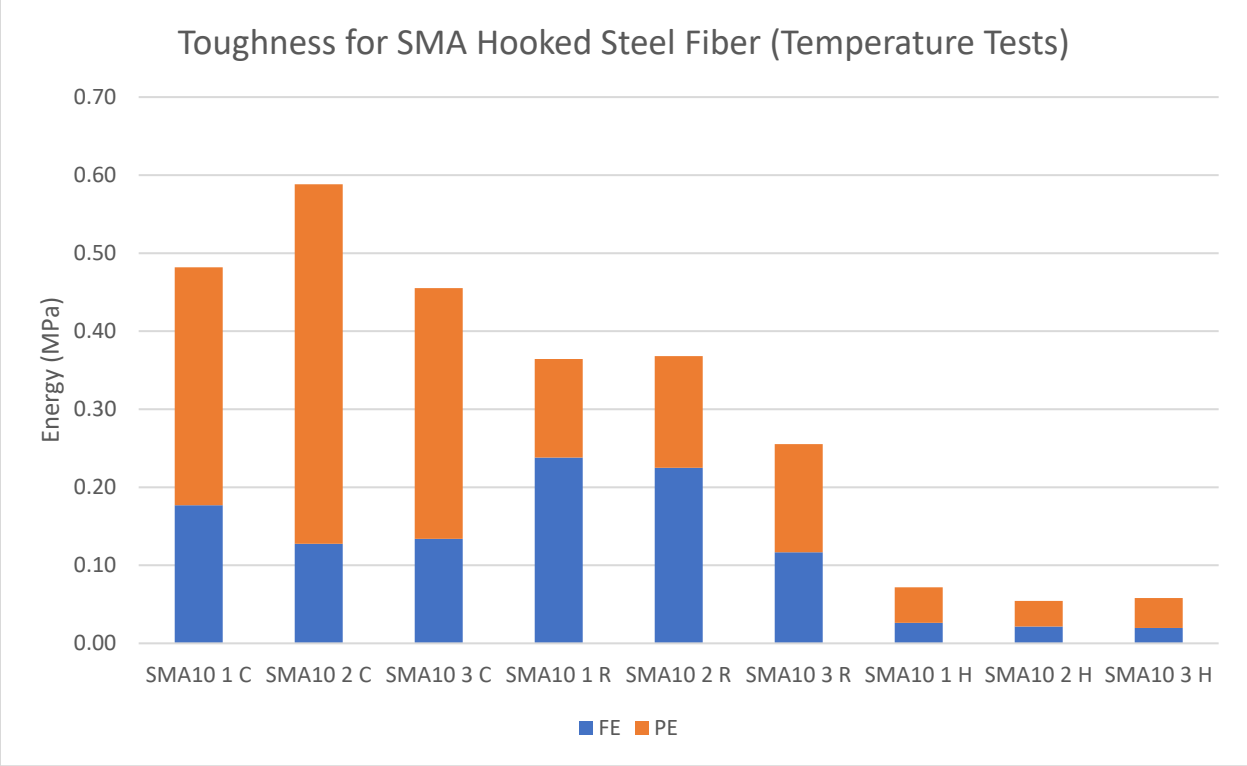

Figure 4.13: Toughness of SMA FRAC under different temperatures.

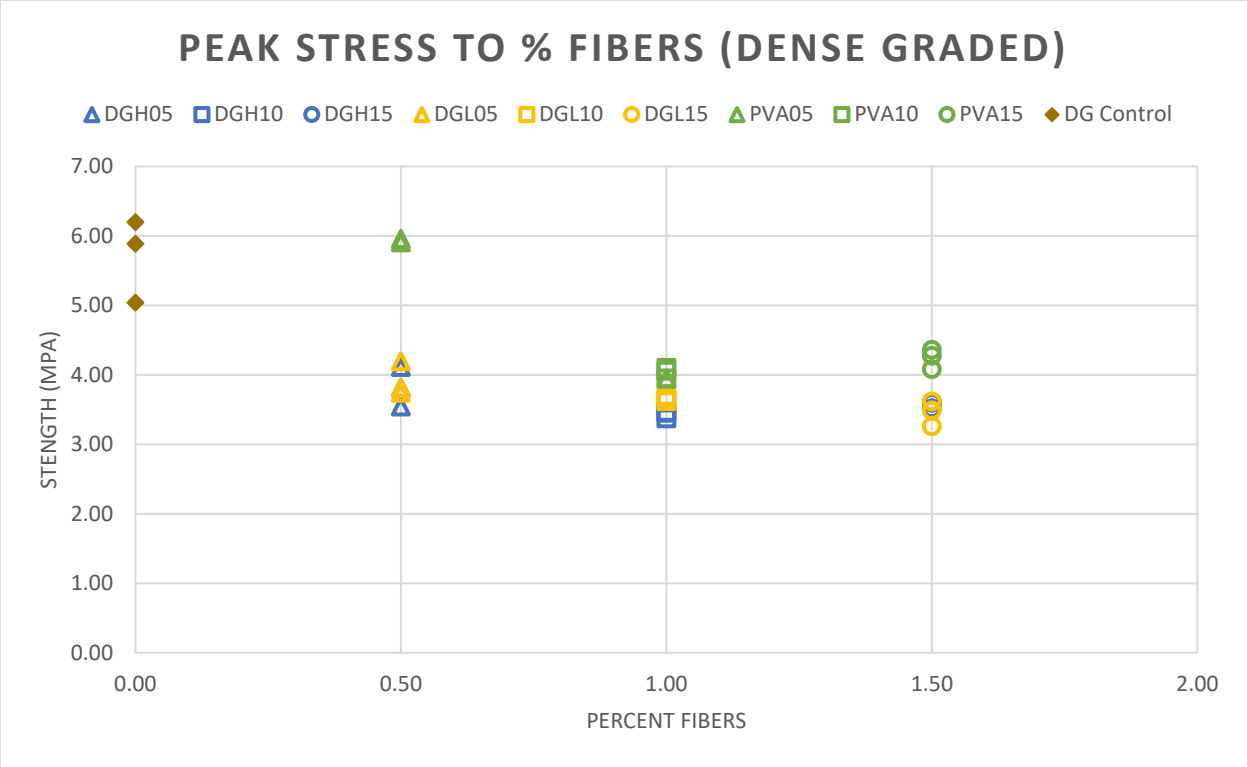

Figure 4.14: Peak stress to Fibers (DG).

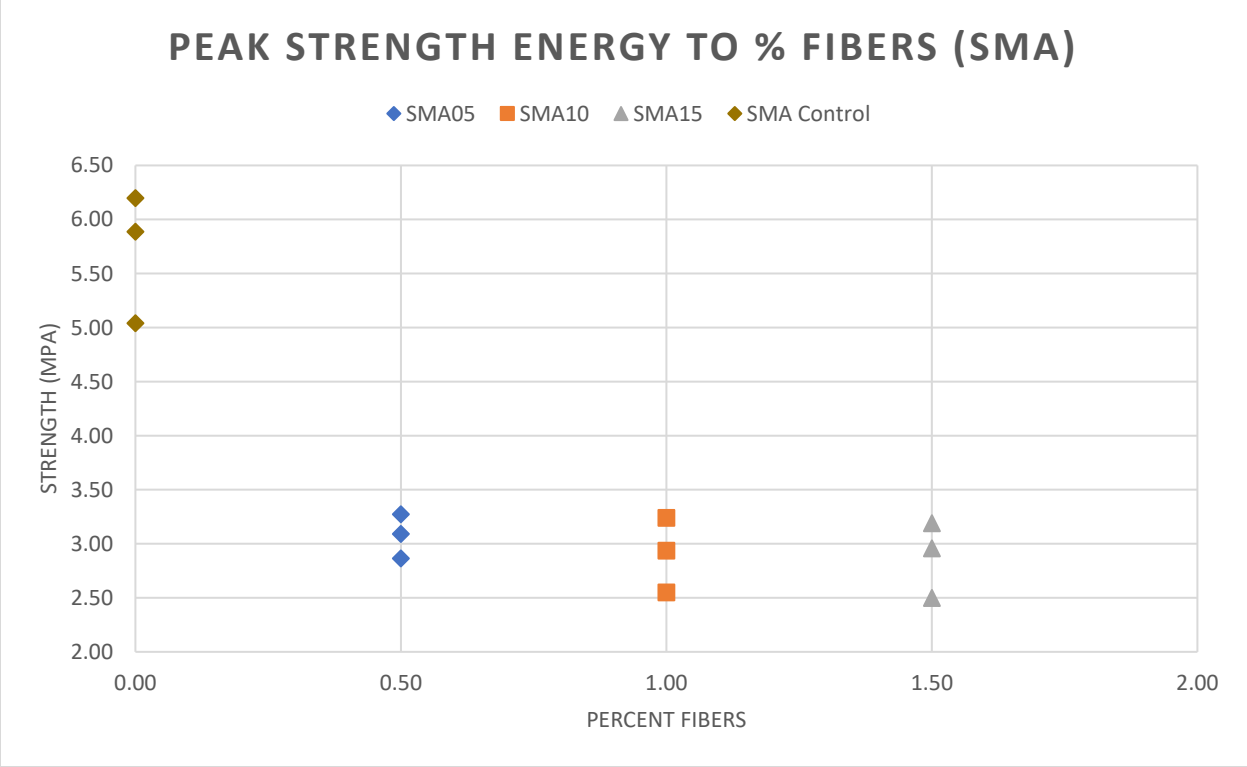

Figure 4.15: Peak stress to Fibers (SMA).

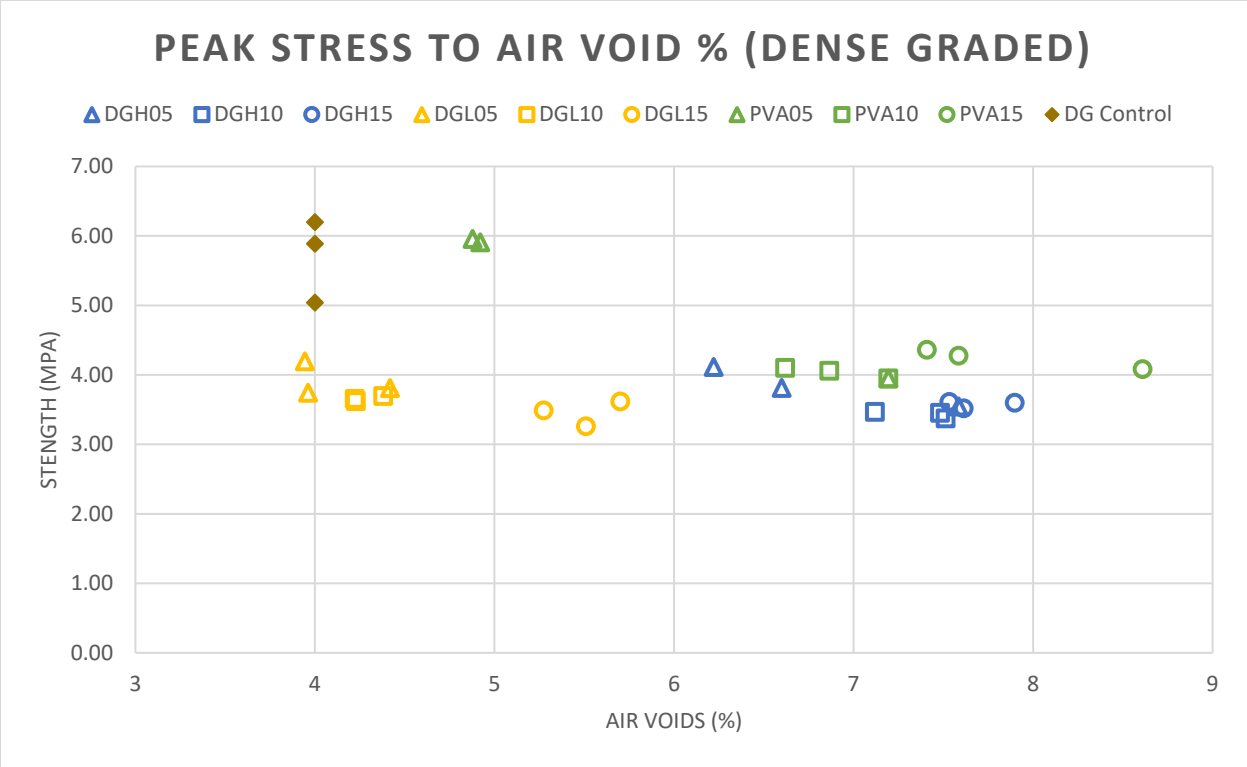

Figure 4.16: Peak stress to Air Voids (DG).

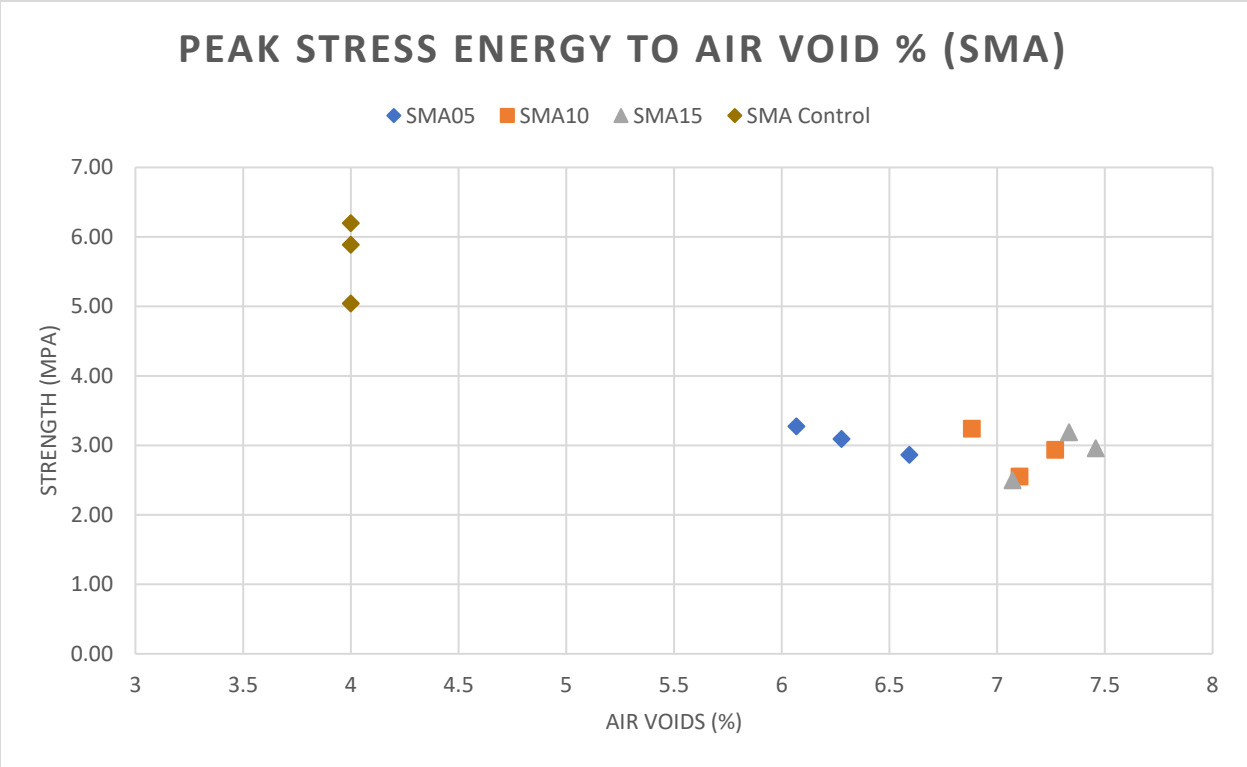

Figure 4.17: Peak stress to Air Voids (SMA).

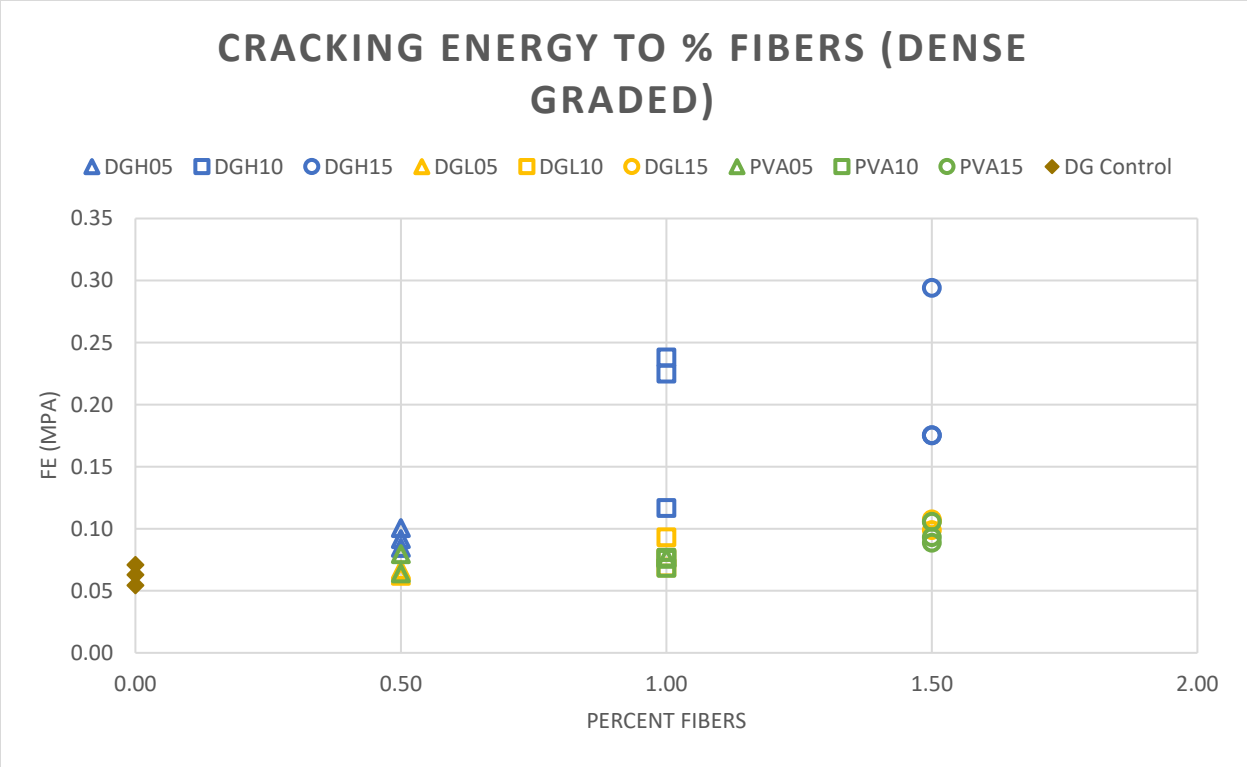

Figure 4.18: Cracking Energy to % Fibers DG.

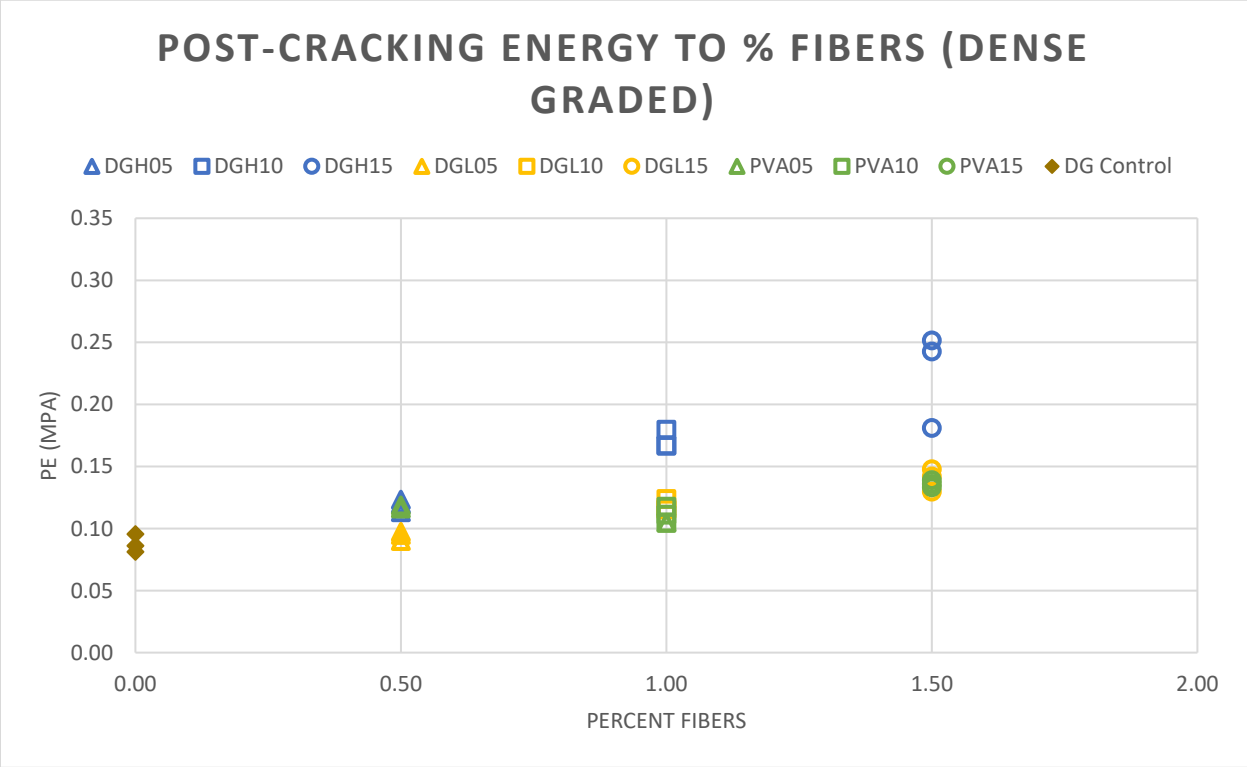

Figure 4.19: Post-Cracking energy to % Fibers DG.

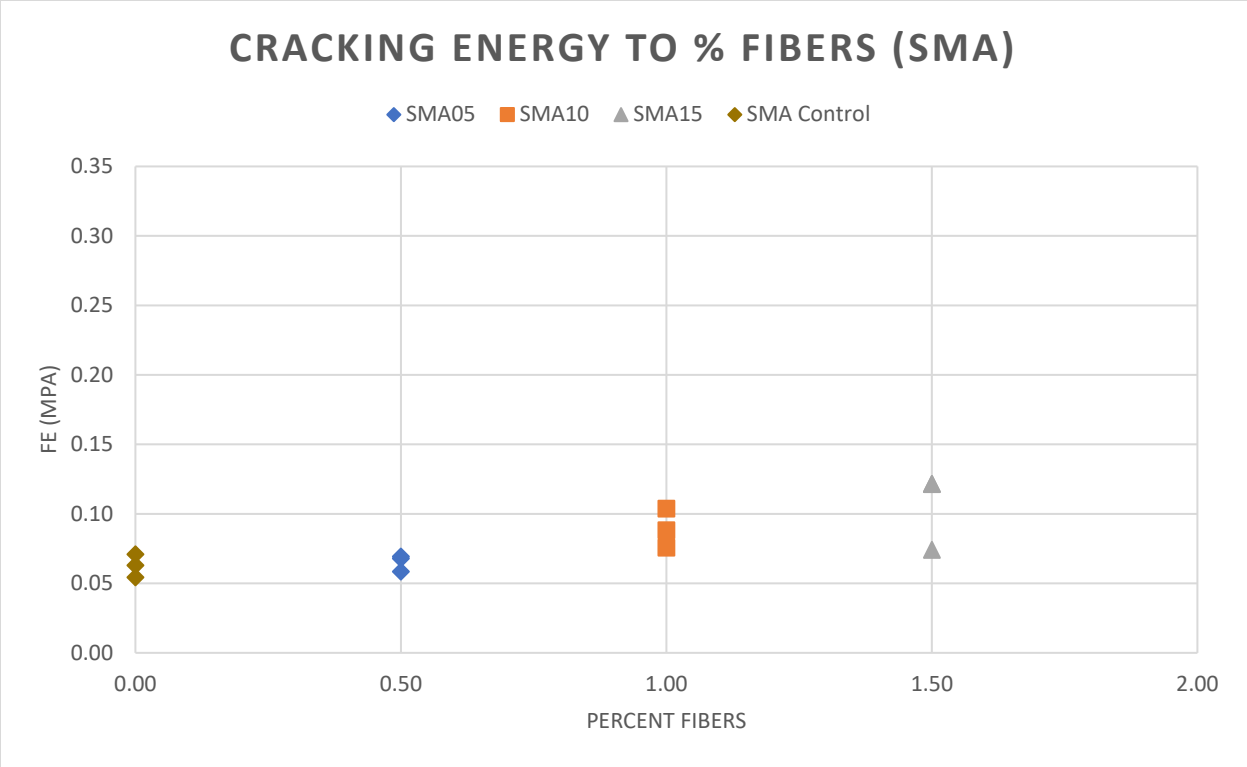

Figure 4.20: Cracking Energy to % Fibers SMA.

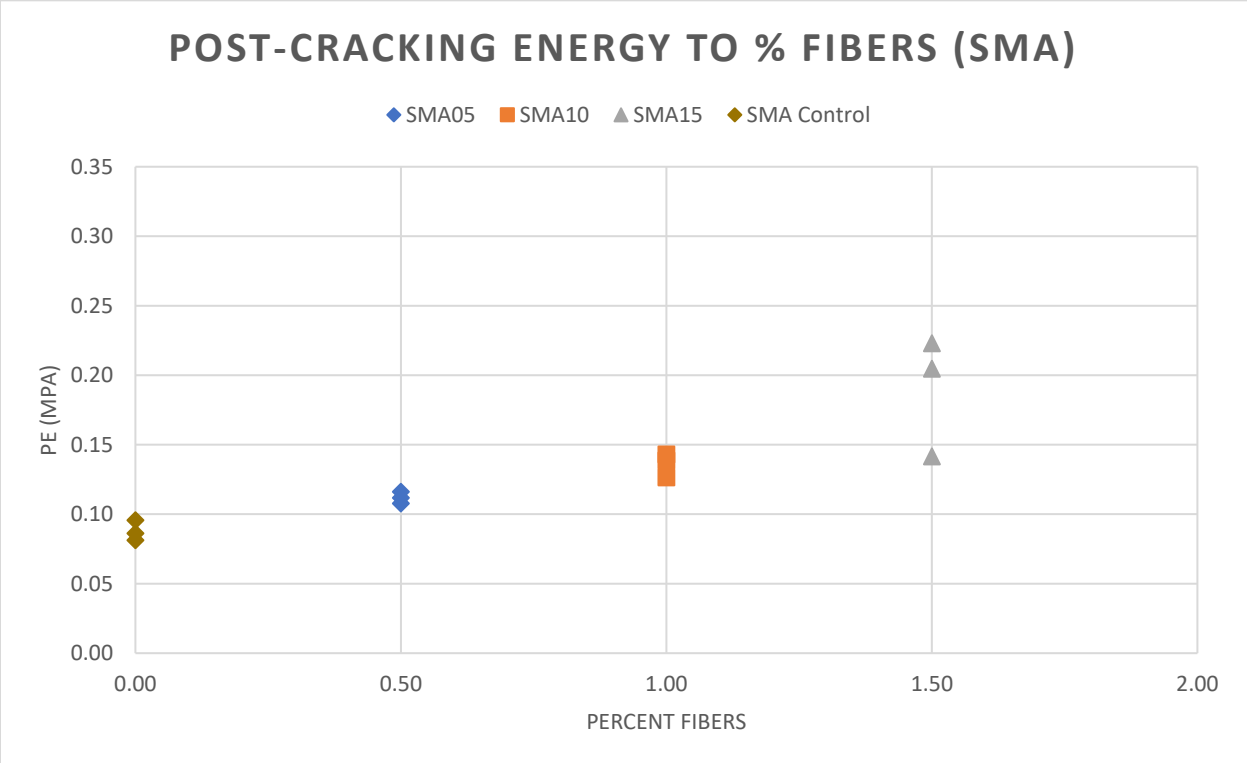

Figure 4.21: Post-Cracking energy to % Fibers SMA.

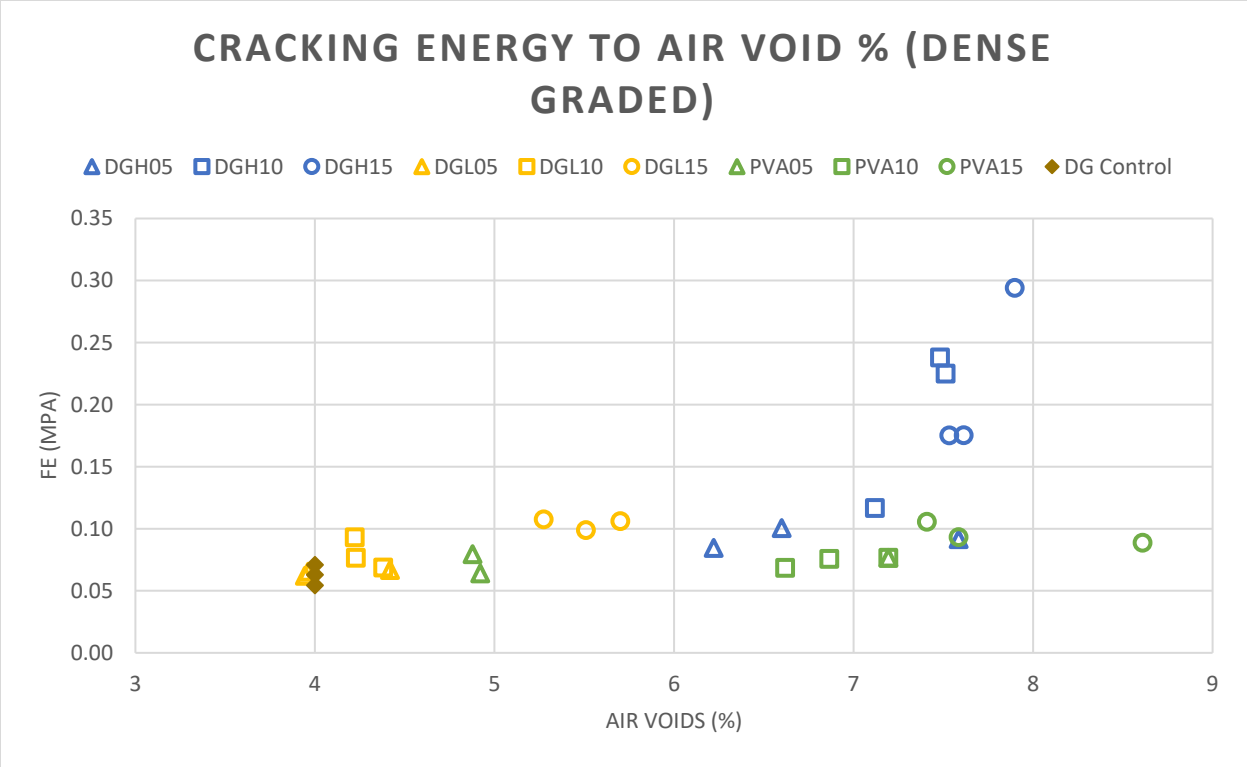

Figure 4.22: Cracking Energy to Air Voids % DG.

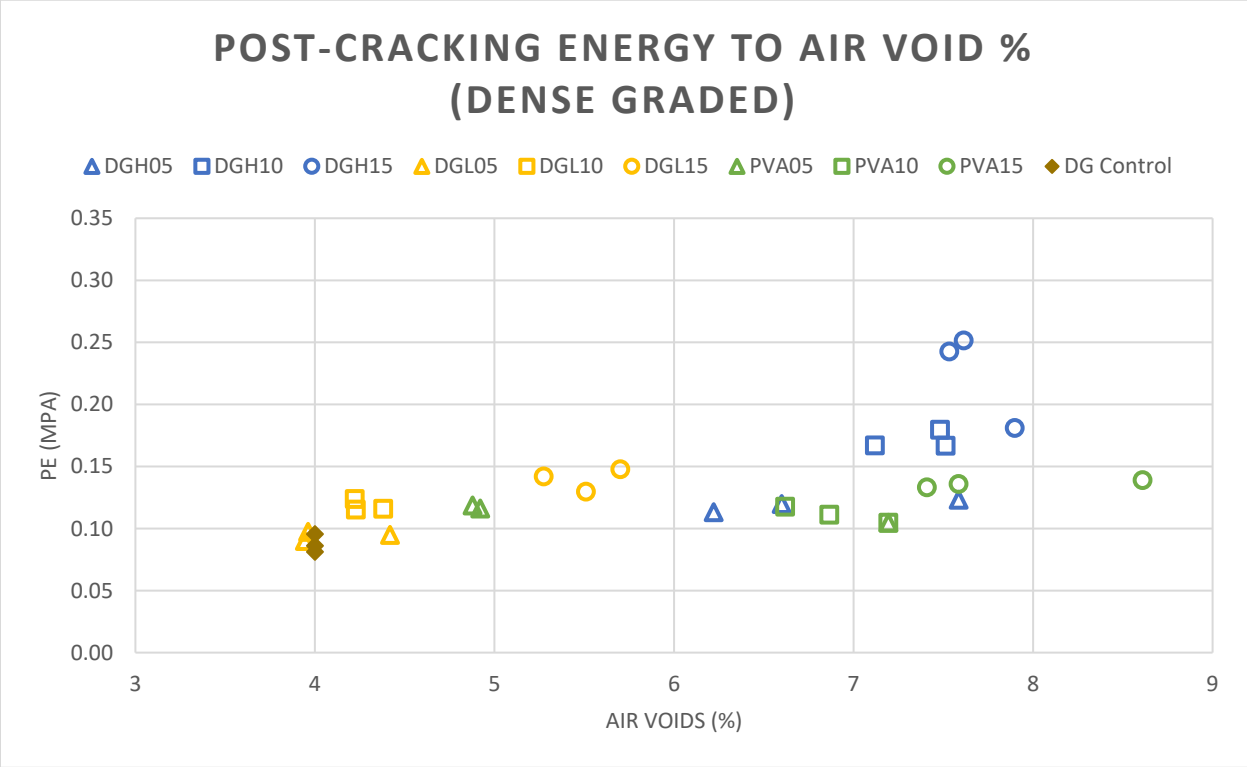

Figure 4.23: Post-Cracking energy to Air Voids % DG.

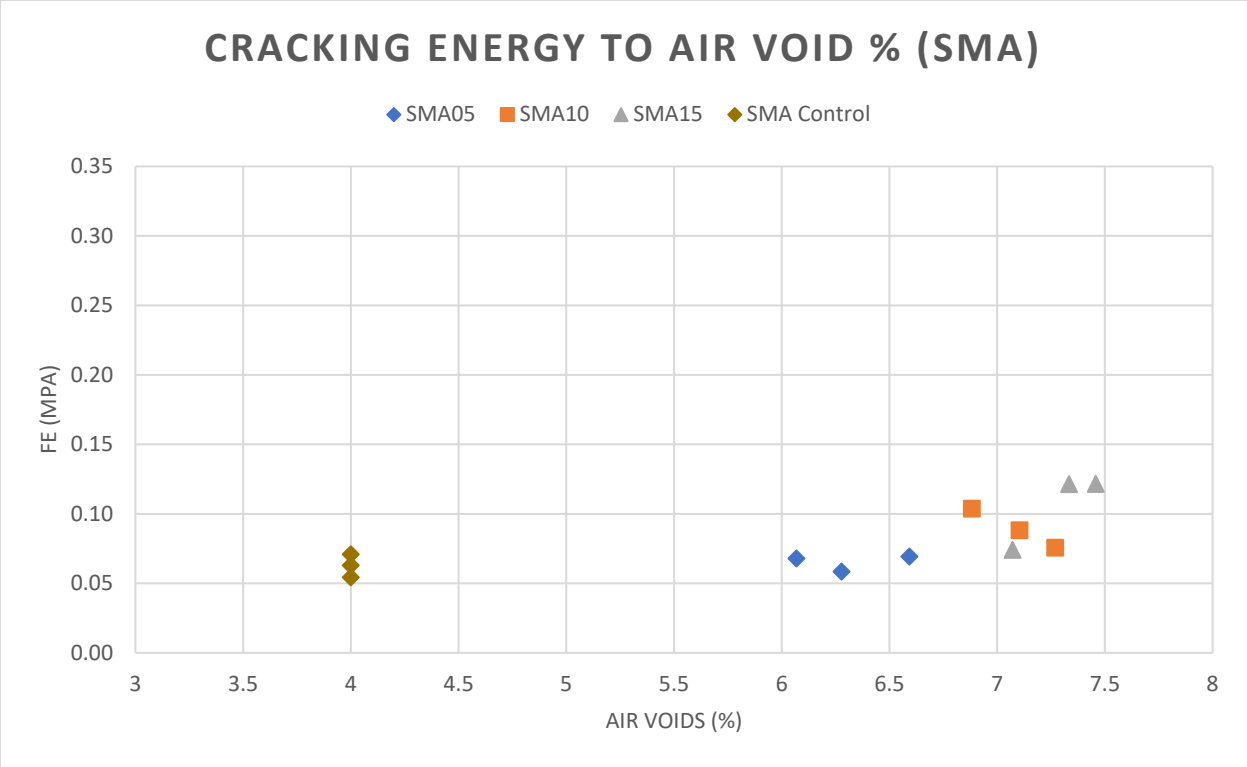

Figure 4.24: Cracking Energy to Air Voids % SMA.

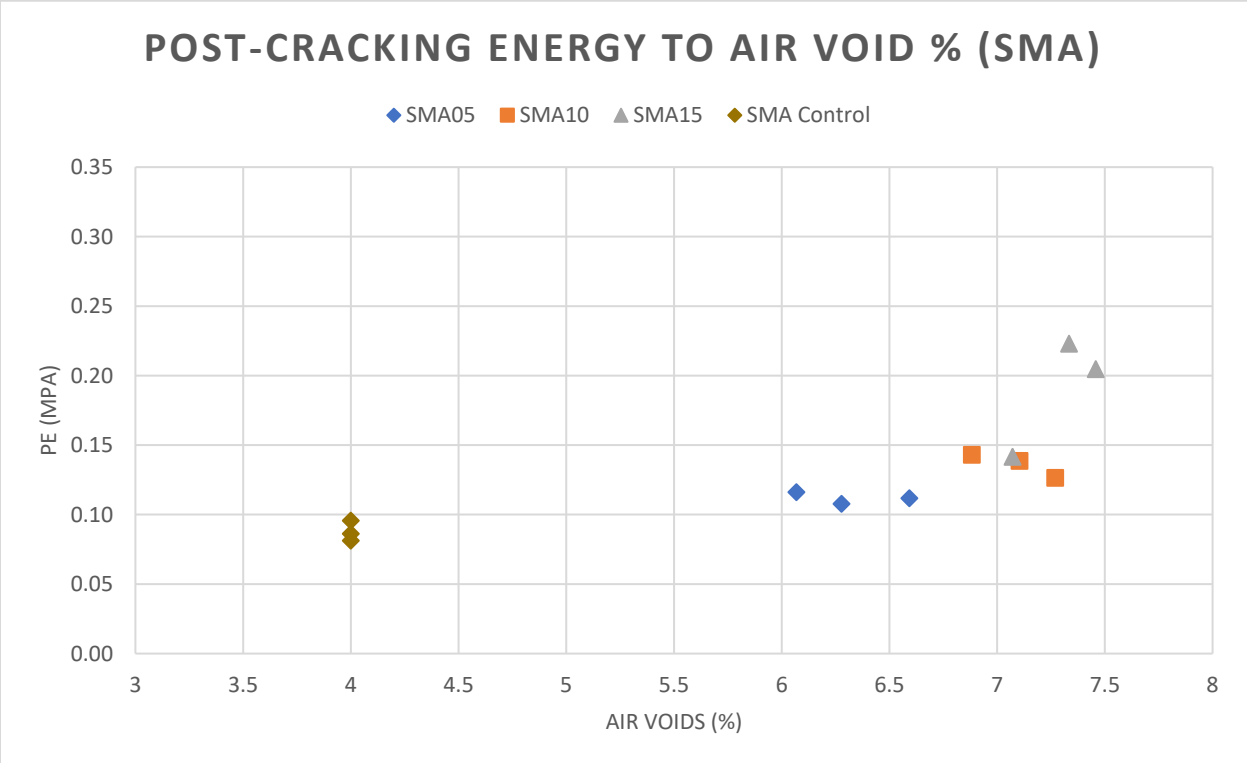

Figure 4.25: Post-Cracking energy to Air Voids % SMA.

FE and PE were obtained from the results given from the MTS. Figure 4.2 to 4.5 show the stress strain curves of the asphalt specimens. The area under the curve prior to reaching its peak stress defines the material's Cracking energy. Post-Cracking Energy is measure from the same Figures and curves. The distance from zero to the location of the peak energy in the strain is defined as Strain_p in Table 4.1. To measure PE, the value of Strain_p is multiplied by 2 and the area under the curve starting from Strain_p to 2Strain_P is used to measure PE. Table 4.1 depicts the values of sthe strength at Strain_p, 2Strain_p, FE, PE, and even the specific air voids within that particular specimen. Strees_p is the peak stress, while Stress_f is the stress at 2Strain_p. Figure 4.18 is a Figureic representing the values of PE and FE as shown in Park et al. (2015).

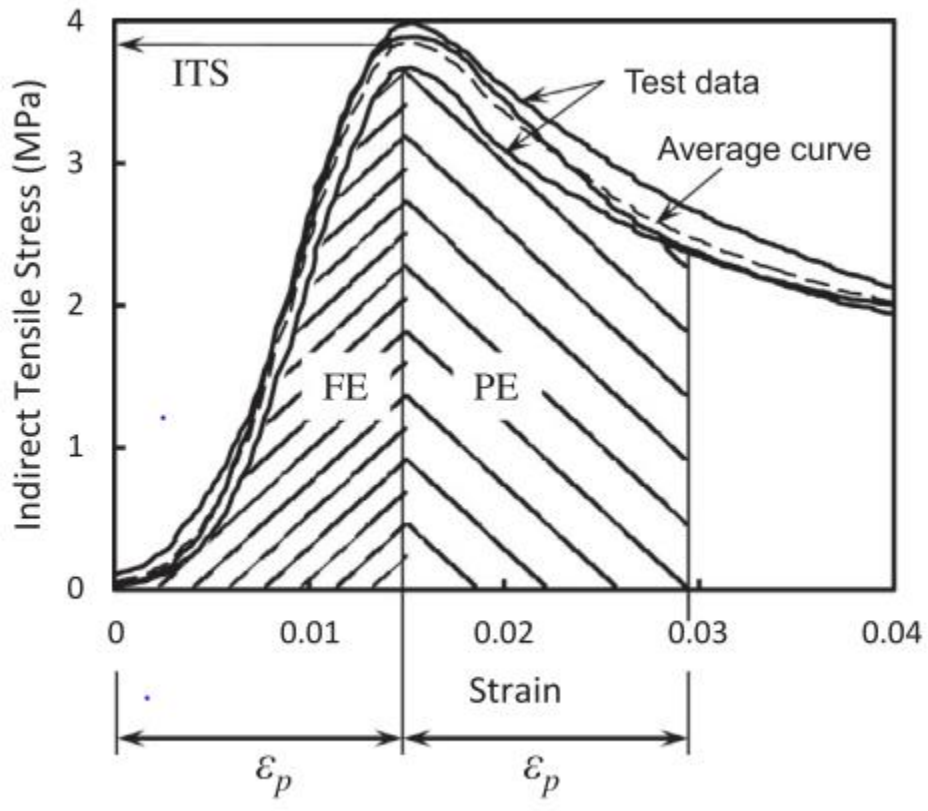

Figure 4.26: Cracking energy, and Post-Cracing Energy (Park et al. 2015).

Figure 4.1 show the cummulative amount of air voids within the fiber reinforced specimens. Figures 4.8 to 4.13 visually compare the FE and PE of the fiber reinforced specimens to the control specimens. Figures 4.14 and 4.15 compare the peak stress of the specimen to the percent by volume of fibers used in those specimens. Finally, Figures 4.16 to 4.17 compare the peak stress of the speciems to the air voids present in each of the specimens.

Discussion

This experiment attempted to evaluate the effect of fibers by conducting tests that would measure their performance withing the specimen. Fibers within the specimen interacts differently with the aggregate and with the binder. The objective was to improve this interaction with the aggregate causing a fiber-aggregate interlocking and creating the bridging effect that was previously discussed. However, in the presence of binder, there will always be adhesion between the fiber and binder. Thus, when evaluating the results, it is very difficult to evaluate just the fiber-aggregate interlocking. There are several factors that affected the strength of the binder in this experiment. Some of these factors is the quantity of binder used, the number of gyrations (compactions) applied, percent air voids, and percent fibers. All samples were prepared the same with no order or any different techniques. The only difference is that when mixing aggregate, fibers were introduced to ensure optimum dispersion. Each of the Figures that were shown in the previous section will be discussed. Initial expectations and performances will be evaluated.

Figure 4.1 has results that matched initial expectations. Previous research had analyzed the impact of fibers of the air voids. It was expected that when 0.5% fibers are introduced, air voids would substantially increase, when that value reached 1.0%, another substantial increase

was expected. However, after adding more fibers there would be a point where the air voids would not increase by much more. A plateau after 1.0% fibers was expected, and at 1.5% fibers, there was a relatively low increment of air voids, except in the Large Hooked Steel fibers and in PVA fibers. Because of the size and density, PVA and the Large Hooked Steel fibers did not have large quantities present, so it is estimated that this plateau would be present at larger quantities.

Figure 4.2 shows the Strain Stress curve for the DG Hooked Steel fibers at the 3 different percentages and the control specimens. This Figure shows an initial patterns and effects of fibers that can be observed in the next following Figures. There appears to be a counterbalance between the benefits and the drawbacks from using fibers in asphalt concrete. The presence of fibers has proven to improve the peak stress of the material; however, this Figure shows that the presence of fibers significantly reduced the peak stress of the material. At 0.5% there is a significant decrease in the peak stress of the material, and when the fibers are increased to 1.0% there is another decrease. At 1.5% there is a slight increase in the peak stress, and this might do with the large quantities of fibers present, however still hindered by the air voids present. This exact same pattern can be observed by the Larger hooked steel fibers as seen in Figure 4.3. However, in this scenario, at 1.5% there is no increase of performance. In the case of the DG PVA fibers, initial quantities seem to have a substantial number of fibers that slightly increased the peak stress of the asphalt specimens. At 1.0 and 1.5% the air voids begin to increase significantly, causing the peak stress of the specimen to decrease. Stone Matrix Asphalt using the hooked steel fibers (Figure 4.5) proved to be rather futile when attempting to increase its peak stress. It is very likely that the fibers used might not have been thick or long enough to create a bridging effect within the aggregate, however it would introduce air voids causing the material to act unpredictably.

Figures 4.8 to 4.11 shows the toughness of each of the samples. Toughness is obtain by adding the FE and PE of each of the samples. Similarly, Figure 4.8 demonstrates a pattern that can be observed in Figures 4.9 to 4.11. In all cases adding fibers increases the material's overall toughness and shows an imporvement over the control samples. This can be seen in particular when using the smaller hooked steelf fibers. PVA and the large hooked steel fibers definetely improve over the control specimens but the addition of fibers did bery little to improve toughnes. In the case of the DG PVA and the large hooked steel fibers, there is a particlualry larger increase when there is a 1.5% fibers. It is very likely that the quantity of fibers played a significant role in improving the material toughness.

Figures 4.14 to 4.17 compares the peak stress to important parameters, such as air voids and percent fibers. In Figure 4.14 the best performing specimens were the DG PVA fibers at 0.5%. while the worst performing specimens were the DG large hooked steel at 1.5% fibers. In Figure 4.15 the stone matric seem to be very even with the SMA with 0.5% of the hookes steel fibers slight performing better than the SMA at 1.0%. The same patterns can be observed when comparing the peak stress to the percent fibers as seen in Figures 4.16 and 4.17.

Figures 4.18 to 4.25 discuss how the air voids and the percent fibers impact the cracking energy and post cracking energy. Figure 4.18 to 4.21 overall show the same pattern throughout. This shows how the addition of fibers was able to increase the FE and PE of the Asphalt. This mirrors previous results showing that the asphalt with higher reinforcement was able to increase the oveall toughness of the material. When analyzing the impact of air voids to the FE and PE as seen in Figure 4.21 to 4.25, it is difficult to to come up to the conclusion of its direct impact on these factors. However, the samples with the most fibers did create the most air voids, and as a result, it does appear that the increment of air voids increases the FE and PE.

Figures 4.6, 4.7, 4.12, and 4.13 analyze the impact that temperature changes have on the fibers and the asphalt specimens. Figure 4.6 and 4.7 show how temperature changes impact the overall toughness of the asphalt. Changing the specimens temperature proceeded as expected. Colder temperature resulted in a stiffer binder, and it also resulted in a higher toughness than without fibers at room temperature this can be seen in Figure 4.12 and 4.13. Under colder temperature it was expected to have a higher peak strenght and low toughness. Under low temperatures the FRAC behaved as expected, low temperatures resulted in more compliant binder and fibers.

The results obtained allign with the preliminary air void tests. The effects of air voids were believed to be minimal. The addition of fibers was expected to increase the amount of air voids present. It was hypothesized that this addition of air voids would be outweigh by the benefits of that are obtained from using fibers. However, because of this the peak stresss of the fibers were significantly reduced. The addition of fibers however did present the benefits in improving the toughness of the material. Toughness refers the the ability of the material to be able to ablsorb energy and deform without fracturing. In every case the presense of fibers had a significant role in improving this. The fibers were able to redistribute the forces applied and allowed the material to deform more withough completely failing. The benefits of fibers can significantly increase the life cycle of the road. Overall the DG Smaller Hooked steel improved the material's toughness, and this might be due to the quantity of the fibers and the materials gradation. Smaller aggregates and smaller fibers allowed the transfering of loads throughout the specimen. The larger steel fiber and the PVA did benefit, but because of the lack of fibers, there was no significant increase in performance. SMA with the smaller hooked steel fibers preformed somewhat similar to the Desne Graded, but the larger aggregate and the particular size of fiber

might not have been optimal. Additionally, SMA had a significantly more amount of binder, wich most likely hindered the interlocking mechanism. Finally, the fibers were able to privide additional toughness to both DG and SMA under a brittle environment, meaning that it could be useful under colder climate conditions.

Previous literature had identified the improvement of the material's toughness and was able to withstand higher loads. This experiment was able to identify the improvement in toughness. Other experiments were very likely to increase the number of compactions given in the asphalt samples to minimize the negative effects that air voids have in the asphalt. The effects of air voids were underestimated, however the benefits of fibers were still present.

CHAPTER V

CONCLUSIONS AND FUTURE WORK

Aiming to understand the fiber-particle interactions in fiber reinforced asphalt concrete, a series of compression tests were conducted in this study for some selected cases. The specimens with two aggregate gradations (dense graded and gap graded with NMAS 19 mm) were prepared and three fiber types (30 mm steel, 40 mm steel, and 30 mm PVA fibers) were used. Full stress-strain curves were obtained under constant crosshead rate tests of 1 mm/minute compressive loading rate.

The results show that adding fibers increases air voids. Correspondingly the compressive strengths and stiffnesses of fiber reinforced specimens measured at 20 °C were lower than the control (unreinforced) specimens. Because of the low stiffnesses of the fiber reinforced specimens, the peak (maximum) stresses appear at higher strains than control specimens. On the other hand, the cracking energy (FE) and post-cracking energy (PE) were higher in fiber reinforced specimens. These behaviors were observed in both dense graded and gap graded mixtures.

It is difficult to conclude whether the reduced strengths of fiber reinforced specimens were caused by the increased air void or by adding fibers. In addition, there is a possibility of strength improvements when different fiber selection. To clarify these, further investigations will beneeded.

REFERENCES

Abtahi, S. M., Sheikhzadeh, M., and Hejazi, S. M. (2010). "Fiber-reinforced asphalt-concrete–a review." *Construction and Building Materials*, 24(6), 871-877.

Alfalah, A., Offenbacker, D., Ali, A., DeCarlo, C., Lein, W., Mehta, Y., and Elshaer, M. (2020). "Assessment of the Impact of Fiber Types on the Performance of Fiber-Reinforced Hot Mix Asphalt." *Transportation Research Record: Journal of the Transportation Research Board*, 2674, 036119812091242.

Alfalah, A., Offenbacker, D., Ali, A., Mehta, Y., Elshaer, M., and Decarlo, C. (2021). "Evaluating the impact of fiber type and dosage rate on laboratory performance of Fiber-Reinforced asphalt mixtures." *Construction and Building Materials*, 310, 125217.

Behbahani, H., Nowbakht, S., Fazaeli, H., and Rahmani, J. (2009). "Effects of fiber type and content on the rutting performance of stone matrix asphalt." *Journal of applied sciences*, 9(10), 1980-1984.

Cetin, A., Evirgen, B., Karslioglu, A., and Tuncan, A. (2021). "The effect of basalt fiber on the performance of stone mastic asphalt." *Periodica Polytechnica Civil Engineering*, 65(1), 299-308.

Chen, H., Xu, Q., Chen, S., and Zhang, Z. (2009). "Evaluation and design of fiber-reinforced asphalt mixtures." *Materials & Design*, 30(7), 2595-2603

Enieb, M., Diab, A., and Yang, X. (2021). "Short-and long-term properties of glass fiber reinforced asphalt mixtures." *International Journal of Pavement Engineering*, 22(1), 64-76.

Gao, H., Zhang, L., Zhang, D., Ji, T., and Song, J. (2021). "Mechanical properties of fiber-reinforced asphalt concrete: Finite element simulation and experimental study." *e-Polymers*, 21(1), 533-548.

Gu, Q., Kang, A., Li, B., Xiao, P., and Ding, H. (2022). "Effect of fiber characteristic parameters on the high and low temperature rheological properties of basalt fiber modified asphalt mortar." *Case Studies in Construction Materials*, 17, e01247.

Gu, X., Xu, T., and Ni, F. (2014). "Rheological Behavior of Basalt Fiber Reinforced Asphalt Mastic." *Journal of Wuhan University of Technology-Mater. Sci. Ed.*, 29, 950-955

Guo, F., Li, R., Lu, S., Bi, Y., and He, H. (2020). "Evaluation of the effect of fiber type, length, and content on asphalt properties and asphalt mixture performance." *Materials*, 13(7), 1556.

Guo, J. F. (2014). "The Effect of Steel Fiber on the Road Performence of Asphalt Concrete." *Applied Mechanics and Materials*, 584-586, 1342-1345.

Guo, Q., Wang, H., Gao, Y., Jiao, Y., Liu, F., and Dong, Z. (2020). "Investigation of the low-temperature properties and cracking resistance of fiber-reinforced asphalt concrete using the DIC technique." *Engineering Fracture Mechanics*, 229, 106951.

Ige, O., Barnett, S., Chiverton, J., Nassif, A., and Williams, J. (2017). "Effects of steel fibre-aggregate interaction on mechanical behaviour of steel fibre reinforced concrete." *Advances in Applied Ceramics*, 116(4), 193-198.

Jenq, Y.-S., Liaw, C.-J., and Lieu, P. (1993). "Analysis of crack resistance of asphalt concrete overlays--a fracture mechanics approach." *Transportation Research Record*(1388).

Keya, K., Kona, N. A., Koly, F. A., Maraz, K. M., Islam, M. N., and Khan, R. A. (2019). "Natural fiber reinforced polymer composites: history, types, advantages, and applications." *Materials Engineering Research*.

Kim, M.-J., Kim, S., Yoo, D.-Y., and Shin, H.-O. (2018). "Enhancing mechanical properties of asphalt concrete using synthetic fibers." *Construction and Building Materials*, 178, 233-243.

Liu, Q., Li, B., Schlangen, E., Sun, Y., and Wu, S. (2017). "Research on the mechanical, thermal, induction heating and healing properties of steel slag/steel fibers composite asphalt mixture." *Applied sciences*, 7(10), 1088.

Liu, Z., Wang, Y., Meng, Y., Han, Z., and Jin, T. (2021). "Comprehensive performance evaluation of steel fiber-reinforced asphalt mixture for induction heating." *International Journal of Pavement Engineering*, 1-12.

Lou, K., Wu, X., Xiao, P., Kang, A., Wu, Z., and Xia, Y. (2021). "Comprehensive study about effect of basalt fiber, gradation, nominal maximum aggregate size and asphalt on the anti-cracking ability of asphalt mixtures." *Applied Sciences*, 11(5), 2289.

Lou, K., Xiao, P., Kang, A., Wu, Z., and Lu, P. (2020). "Suitability of fiber lengths for hot mix asphalt with different nominal maximum aggregate size: A pilot experimental investigation." *Materials*, 13(17), 3685.

Mahrez, A., Karim, M. R., and Katman, H. Y. b. (2005). "FATIGUE AND DEFORMATION PROPERTIES OF GLASS FIBER REINFORCED BITUMINOUS MIXES." *Journal of the Eastern Asia Society for Transportation Studies*, 6, 997-1007.

Mashaan, N., Karim, M., Khodary, F., Saboo, N., and Milad, A. (2021). "Bituminous Pavement Reinforcement with Fiber: A Review." *CivilEng*, 2(3), 599-611.

Miao, Y., Wang, T., and Wang, L. (2019). "Influences of interface properties on the performance of fiber-reinforced asphalt binder." *Polymers*, 11(3), 542.

Mohammed, M., Parry, T., Thom, N., and Grenfell, J. (2018). "Investigation into the bond strength of bitumen-fibre mastic." *Construction and Building Materials*, 190, 382-391.

Motamedi, H., Fazaeli, H., Aliha, M., and Amiri, H. R. (2020). "Evaluation of temperature and loading rate effect on fracture toughness of fiber reinforced asphalt mixture using edge notched disc bend (ENDB) specimen." *Construction and Building Materials*, 234, 117365.

Muftah, A., Bahadori, A., Bayomy, F., and Kassem, E. (2017). "Fiber-Reinforced Hot-Mix Asphalt: Idaho Case Study." *Transportation Research Record*, 2633(1), 98-107.

Noorvand, H., Mamlouk, M., and Kaloush, K. (2022). "Evaluation of Optimum Fiber Length in Fiber-Reinforced Asphalt Concrete." *Journal of Materials in Civil Engineering*, 34(3), 04021494.

Noorvand, H., Salim, R., Medina, J., Stempihar, J., and Underwood, B. S. (2018). "Effect of synthetic fiber state on mechanical performance of fiber reinforced asphalt concrete." *Transportation Research Record*, 2672(28), 42-51.

Park, P., El-Tawil, S., and Naaman, A. E. (2017). "Pull-out behavior of straight steel fibers from asphalt binder." *Construction and Building Materials*, 144, 125-137.

Park, P., El-Tawil, S., Park, S.-Y., and Naaman, A. E. (2015). "Cracking resistance of fiber reinforced asphalt concrete at −20°C." *Construction and Building Materials*, 81, 47-57.

Pei, Z., Lou, K., Kong, H., Wu, B., Wu, X., Xiao, P., and Qi, Y. (2021). "Effects of Fiber Diameter on Crack Resistance of Asphalt Mixtures Reinforced by Basalt Fibers Based on Digital Image Correlation Technology." *Materials (Basel)*, 14(23).

Serin, S., Morova, N., Saltan, M., and Terzi, S. (2012). "Investigation of usability of steel fibers in asphalt concrete mixtures." *Construction and Building Materials*, 36, 238-244.

Slebi-Acevedo, C. J., Lastra-Gonzalez, P., Castro-Fresno, D., and Bueno, M. (2020). "An experimental laboratory study of fiber-reinforced asphalt mortars with polyolefin-aramid and polyacrylonitrile fibers." *Construction and Building Materials*, 248, 118622.

Slebi-Acevedo, C. J., Lastra-González, P., Pascual-Muñoz, P., and Castro-Fresno, D. (2019). "Mechanical performance of fibers in hot mix asphalt: A review." *Construction and Building Materials*, 200, 756-769.

Stempihar, J. J., Souliman, M. I., and Kaloush, K. E. (2012). "Fiber-reinforced asphalt concrete as sustainable paving material for airfields." *Transportation research record*, 2266(1), 60-68.

T-84, A. A. S. H. T. O. (2022). "Standard Method of Test for Specific Gravity and Absorption of Fine Aggregate." 11.

T-85, A. A. S. H. T. O. (2022). "Standard Method of Test for Specific Gravity and Absorption of Coarse Aggregate." 11.

T-166, A. A. S. H. T. O. (2022). "Standard Method of Test for Bulk Specific Gravity (Gmb) of Compacted Asphalt Mixtures Using Saturated Surface-Dry Specimens." 8.

T-209, A. A. S. H. T. O. (2022). "Standard Method of Test for Theoretical Maximum Specific Gravity (Gmm) and Density of Asphalt Mixtures." 11.

T-269, A. A. S. H. T. O. (2014). "Standard Method of Test for Percent Air Voids in Compacted Dense and Open Asphalt Mixtures." 5.

T-312, A. A. S. H. T. O. (2022). "Standard Method of Test for Preparing and Determining the Density of Asphalt Mixture Specimens by Means of the Superpave Gyratory Compactor." 14.

Tahenni, T., Chemrouk, M., and Lecompte, T. (2016). "Effect of steel fibers on the shear behavior of high strength concrete beams." *Construction and Building Materials*, 105, 14-28.

Takaikaew, T., Tepsriha, P., Horpibulsuk, S., Hoy, M., Kaloush, K. E., and Arulrajah, A. (2018). "Performance of fiber-reinforced asphalt concretes with various asphalt binders in Thailand." *J. Mater. Civ. Eng*, 30(8), 04018193.

Vargas-Neumann, J., Bariola, J., Blondet, M., and Mehta, P. (1986). "Seismic strength of adobe masonry." *Materials and Structures*, 19, 253-258.

Wang, H., Yang, Z., Zhan, S., Ding, L., and Jin, K. (2018). "Fatigue performance and model of polyacrylonitrile fiber reinforced asphalt mixture." *Applied Sciences*, 8(10), 1818.

Xu, Q., Chen, H., and Prozzi, J. A. (2010). "Performance of fiber reinforced asphalt concrete under environmental temperature and water effects." *Construction and Building Materials*, 24(10), 2003-2010.

Yang, J.-M., Kim, J.-K., and Yoo, D.-Y. (2016). "Effects of amorphous metallic fibers on the properties of asphalt concrete." *Construction and Building Materials*, 128, 176-184.

Yoo, D.-Y., Park, J.-J., and Kim, S.-W. (2017). "Fiber pullout behavior of HPFRCC: Effects of matrix strength and fiber type." *Composite Structures*, 174, 263-276.

Zhang, X., Gu, X., Lv, J., Zhu, Z., and Ni, F. (2018). "Mechanism and behavior of fiber-reinforced asphalt mastic at high temperature." *International Journal of Pavement Engineering*, 19(5), 407-415.

Zheng, Y., Cai, Y., Zhang, G., and Fang, H. (2014). "Fatigue property of basalt fiber-modified asphalt mixture under complicated environment." *Journal of Wuhan University of Technology-Mater. Sci. Ed.*, 29(5), 996-1004.

Ziari, H., Aliha, M., Moniri, A., and Saghafi, Y. (2020). "Crack resistance of hot mix asphalt containing different percentages of reclaimed asphalt pavement and glass fiber." *Construction and Building Materials*, 230, 117015.

Zube, E. (1956). "WIRE MESH REINFORCEMENT IN BITUMINOUS RESURFACING." *Highway Research Board Bulletin* (131), 17.

BIOGRAPHICAL SKETCH

Franher Daniel Cantu Graduated from The University of Texas Rio Grande Valley in December of 2020 with a B.A. in Civil Engineering. He obtained his Fundumentals of Engineering (FE) liscense in September of 2021. He graduated from The University of Texas Rio Grande Valley with a M.S. in Civil Engineering with a specialization in Strucutral Engineering on December of 2022. Franher can be reached at franherdancan@gmail.com.